MINISTRY OF DEFENCE

AERONAUTICAL RESEARCH COUNCIL
REPORTS AND MEMORANDA

The Two-Dimensional Flow Around a Slotted Flap

By D. N. FOSTER, H. P. A. H. IRWIN
and
B. R. WILLIAMS
Aerodynamics Dept., RAE, Farnborough

The Two-Dimensional Flow Around a Slotted Flap

By D. N. FOSTER, H. P. A. H. IRWIN
and
B. R. WILLIAMS
Aerodynamics Dept., RAE, Farnborough

Summary

This Report describes experimental measurements and theoretical analysis of the flow around a wing with a single slotted flap under twodimensional flow conditions. The particular experimental techniques of testing and measurement are described. The results show that the measured flow is strongly dependent on the inviscid solution for the flow around the wing and the flap, and that near to the optimum flap position there is only weak interference between the wake from the wing and the boundary layer on the flap. The reasons for the occurrence of an optimum flap position are described, and some comments made on the influence of Reynolds number on this position.

LIST OF CONTENTS

*Replaces RAE Tech. Report 70164—A.R.C. 32 681.

---

1. Introduction

The single slotted flap has been used on aircraft for many years, and its aerodynamic characteristics were admirably reviewed by Young[1] in 1947. The continuing development of aircraft has led to the demand for more effective flaps, both in respect of increased lift capability, and of decreasing drag contribution. These demands have been met, in part, by the multi-slotted flap. However unless the nature of the flow around the flap is well understood, the development of the shape of the flap, and of the nature and position of any further subdivisions in the flap, must require extensive wind-tunnel tests to achieve worthwhile improvements. Equally, the part that Reynolds number plays in the results measured in low-speed wind tunnels cannot be assessed without an understanding of the flow.

It was to provide an insight of such flows that the work described here was commenced. The ultimate aim was to understand the flow around slotted flaps on swept-back wings. Provided that the wings have not too great a sweep-back ($\leqslant$ 40 degrees) and not too small an aspect ratio ($\geqslant$ 4·5), linearized theory would suggest that there is at least a part of the wing for which the flow may be considered to be similar to that in twodimensional flow. Thus it was decided that the experimental programme would, in the first instance, concentrate on understanding the twodimensional flow around a slotted flap.

The flow characteristics which are measured for a wing and flap result from a complex interaction of multiple lifting surfaces in close proximity, and of their associated boundary layers and wakes. A special problem is that downstream components of the multiple aerofoil have the wakes of the upstream components very close to their upper surfaces. It was appreciated that the effects due to the interactions of the multiple lifting surfaces, and of those due to the viscous layers, could not strictly be separated, but it was considered that an indication of the magnitude of these effects might be possible if one could be calculated in the absence of the other. Work was therefore put in hand to find a suitable theory for the inviscid flow around multiple aerofoils, resulting in the selection of the surface source method due to A. M. O. Smith[2]. It should be noted that this was selected on its performance for single aerofoils, there existing no exact solution for multiple aerofoils.

The corresponding experimental programme commenced in May 1968 with a model of a wing and a single-slotted flap (Fig. 1); a flap deflection of 30 degrees was chosen, since existing test data indicated that the optimum flap position would be well defined at this deflection. In order to allow the combination to achieve lift coefficients similar to those for wing sections with more complex leading-edge devices, a drooped nose was fitted (Fig. 2). A second test series, in May/June 1969, had as its primary aim an investigation of the flow behind a leading-edge slat, and for these tests a flap deflection of 10 degrees was selected in order to avoid overstressing the model. Some measurements were made of the flow around the flap for this leading-edge configuration, and further measurements were obtained, at the same flap deflection, when the slatted leading edge had been replaced by a plain leading edge. The experimental work reported here therefore covers two flap deflections, corresponding approximately to a take-off and a landing configuration, in conjunction with two leading-edge configurations, clean and slatted.

The experimental work was divided into two phases. The first was an investigation of the overall forces, for a wide range of geometric positions of the flap relative to the wing, and the second involved detailed traverses through the viscous layers above the flap· for selected geometric positions of the flap.

2. Details of the Model and Test Facilities

2.1. The Wing.

The wing, which had an unextended chord of 3 ft (0·91 m), was designed to be mounted between the floor and roof turntables of the 13 ft × 9 ft low-speed wind tunnel at R.A.E. Bedford. It consisted basically of a steel framework, to which mouldings of glass reinforced plastic could be bolted to form the contour of the wing, and to which the flap (and slat, when fitted) could be attached. The flap similarly consisted of a steel core and a glass reinforced plastic skin giving the contour shape. The slat was machined from solid metal. The shape of the lower surface of the wing, as originally built, is shown in Fig. 2 for the flap deflected 30 degrees. To remove the discontinuity in slope at $X_w/c_o \simeq 0.6$, for the tests with the flap deflected 10 degrees, a fairing was attached to the model to give the smooth surface shape also shown in Fig. 2.

When mounted in the wind tunnel the deflection of the framework was restrained by two straining wires, shown in Figs. 1 and 3. These wires, mounted in pivots on the axis of rotation of the wing, passed across the working section on the lower surface side of the model, and were fixed to the tunnel structure outside the working section. A strain-gauged link was provided in each wire attachment, to enable the loads carried by the wires to be monitored. The maximum load allowable in each wire was 1000 lbf (4450 N); during the tests the actual load seldom exceeded 500 lbf (2225 N).

The flap was attached to the wing by four brackets, and pivoted about a point below its lower surface, in order to vary the flap deflection. The flap brackets were attached to a jacking mechanism (Fig. 4) mounted off the basic framework. This mechanism allowed the position of the flap to be varied continuously in two directions, parallel to and normal to the chord-line of the wing. The range of movement available was 3 per cent of the chord parallel to the chord-line, and 2 per cent of the chord normal to the chord-line.

The sectional shape of the wing, slat and flap were derived from a basic sectional shape designated RAE 2815*. The flap chord was chosen as 40 per cent of the unextended chord, with the shroud trailing edge being at 87 per cent of the unextended chord. The shape of the flap was decided somewhat arbitrarily, and its coordinates are given in Table 1, together with those of the main wing, in its various configurations, and those of the slat. All coordinates have been nondimensionalised using the unextended chord length.

For the majority of the tests transition was free on all surfaces. A comparative test for the effect of fixing transition was made for the plain leading-edge configuration, with the flap deflected 10 degrees and a gap of 2·5 per cent chord. Transition was fixed by 0·5 in (0·014 c_o) wide bands of 0·008 in (0·20 mm) diameter Ballotini, held on by araldite. The bands were positioned as follows:

Surface		Position: x_W/c_o or x_F/c_o
Wing	Upper	0·060
	Lower	0·078
Flap	Upper	0·065
	Lower	0·020

Detailed pressure distributions were measured at the centreline of the model, and the number of pressure tappings on each component was as follows:

Component		Number of pressure tappings
Slat		25
Main wing	Plain leading-edge	62
	Drooped leading-edge	64
	Slatted leading-edge	55
Flap		34

2.2. Pressure Measurement System.

The main method of measuring pressures was by scanivalves and transducers. For the first test series four scanivalves were available, these being increased to eight for the second test series. The scanivalves

---

*Alternative designations for this section are NPL 3111 and HSA 681 'A'.

were automatically sequenced in a ripple pattern to minimise the time required to take a complete pressure distribution, while allowing the pressure from each port to settle for 0·35 sec before being recorded.

Transducers with ranges of ± 2·5 lb/in² , 5 lb/in² and 7·5 lb/in² (17 kN m⁻² , 34 kN m⁻² and 51 kN m⁻²) were used as appropriate. Every alternative port on the scanivalve was connected to a pressure higher than any expected to be measured, in order to eliminate any effects of hysteresis in the transducer. This interport pressure was normally 1 lb/in² (7 kN m⁻²). The output of the transducers was fed to a digital voltmeter, and coded into a form suitable for punching onto eight track paper tape for subsequent reduction.

2.3. *Method of Avoiding Separation of the Boundary Layer on the Wind-Tunnel Walls.*

In order to achieve as near twodimensional conditions as possible, it was necessary to control the separation of the boundary layer on the roof and floor of the wind tunnel, which would occur at the junction with the wing. Earlier tests on a large chord model with plain leading- and trailing-edge flaps, and boundary-layer control by blowing, had shown[3] that suction through the turntables adjacent to the wing was effective in establishing twodimensional conditions up to the stall. This method was therefore adopted here.

A suction box was set flush into each turntable (Fig. 5). Around the fixed portion of the wing, suction was applied through a series of holes. However for the slat and flap, which could be positioned over a wide area of the suction box, the suction was applied through perforated surfaces. These surfaces were supported against deflection under the suction loads by a lattice of thin plates, these in turn being supported by a thick base plate, with sufficient holes to allow the free passage of air, into the main suction chamber (Fig. 5). The perforated surface was 0·050 in (1·27 mm) thick, and the 0·0655 in (1·67 mm) diameter holes gave an open area ratio of 30 per cent. For any given geometric arrangement of the slat and flap, the major part of the perforated surface was sealed by tape, to leave a strip approximately 0·5 in (12·7 mm) wide immediately adjacent to the surface of the slat, flap or wing.

The suction level into the suction box at each end of the model could be individually adjusted, and a large capacity suction pump (free air delivery 5500 cu ft/min (2·6 m³/s)) was used.

2.4. *The Wake Survey Rig.*

The wake survey rig consisted of a rake mounted such that it could be translated and rotated to align with the wake. Two alternative rakes were used, each consisting of 37 pitot tubes and 10 static tubes. the latter being adjacent to every fourth pitot tube. The smaller rake had the pitot tubes spaced 0·25 in (0·007 chord) apart, and the larger rake had the pitot tubes spaced 0·50 in (0·014 chord) apart. The rakes could be mounted, at the mid-span of the model, on a framework of streamlined tubes (Figs. 1 and 3). The rake could be rotated about the centre pitot tube by an actuator mounted on the framework. In turn the framework could be moved normal to the airstream, the base of the framework sliding in rails, and its position being adjusted by a motor driving a lead screw. Both movements were controlled from outside the wind tunnel.

The track for the framework was installed immediately downstream of the turntable in the floor of the working section, so that the rake was approximately one chord downstream of the trailing edge of the flap.

2.5. *Boundary-Layer Traverse Rig.*

It was considered essential that it should be possible to traverse through the viscous layer at any position around the surface of the wing or flap. This requirement implied that the traverse rig must be mounted external to the model, and thus, in addition to a remotely controlled movement, a position indication, relative to the wing or flap surface, was necessary. The system evolved (Fig. 6) consisted of a double-acting hydraulic jack, and a linear motion potentiometer, whose spring loaded spindle moved simultaneously with the shaft of the jack. The hydraulic oil was pressurised by compressed air, which could be directed to one of two reservoirs to allow the jack to extend or retract.

The alternative pitot tubes which could be mounted on the shaft of the jack are shown in Fig. 6, being either a rectangular tube of 0·008 in (0·2 mm) thickness, or a round pitot tube of 0·0195 in (0·50 mm) outside diameter. A static tube was also available. The pressure in the probe was measured by a special

strain-gauge capsule in the first test series, and by a fused quartz Bourdon pressure gauge in the second test series.

The response of the potentiometer was found to be linear with movement, and the accuracy of measurement of the position of the probe was assessed as 0·002 in (0·05 mm). The touchdown of the pitot (or static) tube on the aerofoil surface was indicated by a 'touch-light' system. Since the surface of the model was non-conducting, it was necessary to paint a thin strip of a silver conducting preparation on it to complete the touchdown circuit. To avoid interfering with the pressure plotting holes, this strip was placed some 3 in (7·6 cm) away from the line of the pressure plotting traverse.

The jack and potentiometer were mounted in a streamline fairing on a 'tripod' of streamline tubes, which could be screwed to the floor turntable at any required position. The direction of traverse was adjusted to be normal to the surface of the wing or flap at the touchdown position.

2.6. Surface Pitot Tubes.

In order to measure the skin friction, the boundary-layer probes shown in Fig. 6 were used as surface pitots for part of the work, the remaining measurements being obtained using the razor blade technique[4]. The static pressure at the point of measurement was taken from the tappings used to find the pressure distribution at the model centreline. The readings from the boundary-layer probe were obtained at about 3 in (7·6 cm) off the centreline, where the strip of conducting paint indicated when the probe touched the surface. The razor blades were positioned carefully over the static holes as shown in Fig. 7. The method used to attach the razor blades to the model surface, and a check on the calibration of the arrangement so obtained, is described in the Appendix.

3. Method of Test and Reduction of Results.
3.1. Control of the Wall Boundary Layer.

The effectiveness of the system for controlling the boundary layer on the wind-tunnel walls was monitored by comparing the flow at the ends of the model, and near to the centreline, as judged by tufts. For every position of the flap, and every angle of incidence, the depression in the suction box at each end of the model was adjusted until the adjacent tufts showed that the flow was attached over the same proportion of the chord as for the flow near the centreline of the model. Previous tests[3] had shown that under these conditions the loading across the span of the model was very nearly uniform.

Fig. 8 shows the pressure coefficient for the depression in the suction boxes, for a typical configuration with the leading edge drooped 10 degrees and the flap deflected 30 degrees. Very low pressures occur on the wing around the drooped leading edge, and even lower pressures are needed in the suction boxes to ensure inflow along the whole length of the suction area. Also shown in Fig. 8 is the total mass flow into both of the suction boxes, given both as the physical quantity (lb/sec) and as a nondimensionalised quantity related to the displacement thickness of the boundary layer on the wind-tunnel wall, when the tunnel is empty.

3.2. Pressure Distribution Around the Wing Section.

On each day during which the pressure measurement system was to be used, and in general prior to taking any measurements, each transducer was calibrated, using an accurate pressure gauge (Midwood manometer) as a standard. For each test configuration and angle of incidence, the tunnel and suction flows were then established, and the surface pressures scanned.

The tests were normally made at a wind speed of 200 ft/sec (61 m/sec), for which the dynamic pressure is 0·33 lb/in^2 (2·2 kN m^{-2}). Even for the lowest range transducer ($\pm$ 2·5 lb/in^2), the quoted accuracy of the transducer, 0·25 per cent of full scale value, could result in the measured value of the dynamic pressure being in error by approximately 2 per cent. If this measured value were then used in the reduction of the surface pressures, all values of the pressure coefficient could be in error by this amount. To avoid this, a value of the dynamic pressure, calculated for the tunnel wind speed, was given to the reduction program. Such a technique was possible, as the wind speed control system maintained the speed constant to within $\pm$ 0·1 per cent for the range of model conditions tested.

6

After reduction to pressure coefficient form, the pressures were integrated, assuming a linear variation between pressure tappings, to give the normal and axial force coefficients for each component. Subsequent resolution, initially relative to the chord-line of the wing, and finally to the direction of the flow at infinity, gave the lift coefficient for the complete aerofoil section. Allowance was made for the effect of solid blockage on the wind speed, but no constraint corrections were included.

3.3. *Wake Drag.*

The pressures at the pitot tubes and static tubes comprising the wake survey rake were measured on the pressure measuring system, and a selection of the pitot pressures, and all of the static pressures, were also connected to a water manometer, to assist in positioning the rake. For each test condition the rake was moved normal to the airstream until the centre of the wake was approximately at the centre of the rake, and the rake was then rotated to align with the mean direction of flow in the wake.

After the pressures at the rake had been reduced to pressure coefficient form, in the same manner as for the surface pressures (Section 3.2 above), a static pressure coefficient corresponding to the position of every pitot tube was derived by linear interpolation between the values corresponding to the adjacent static tubes. The wake drag was then evaluated, using the equation[5]

$$C_D = 2 \int_{\substack{\text{across} \\ \text{wake}}} (\sqrt{C_{p_H} - C_{p_s}})(1 - \sqrt{C_{p_H}}) \, d\left(\frac{z_w}{c_o}\right) \tag{1}$$

where C_{p_H} is the pressure coefficient corresponding to the pitot pressure, and C_{p_s} is the pressure coefficient corresponding to the static pressure.

In the first test series the small number of scanivalves available resulted in the wake pressures and the model surface pressures being measured during separate runs. After reduction to pressure coefficient form, the pressures relevant to the actual wake were selected from those for the complete rake, and the drag evaluated by a separate computer program. In the second test series it was possible to measure the wake pressures simultaneously with the model pressures, and it was considered desirable to be able to evaluate the wake drag in the reduction program. The pitot pressures were measured on $2 \cdot 5$ lb/in^2 transducers, and the analysis outlined in Section 3.2 suggested that unwanted contributions to the wake drag integral would result from values which should have been equal to the freestream pitot pressure, but were low due to the inaccuracy of the transducer. To avoid such errors, it was arranged that the computer program would ignore all contributions to the integral when the value of the term $(1 - \sqrt{C_{p_H}})$ in equation (1) was less than $0 \cdot 012$. For a case where all the pitot pressures are measured correctly, this limit could result in the calculated drag coefficient being in error by a maximum of $0 \cdot 0006$.

3.4. *Traverses through the Viscous Layers.*

During the first test series, which concentrated on the flow over the flap, the rectangular pitot tube (Fig. 6) was used. During the second test series, it was found that the direction of the flow close behind the slat varied markedly across the viscous layer, and it was considered that the rectangular pitot tube would be sensitive to these changes in flow direction. Recourse was therefore made to the round pitot tube (Fig. 6), and this was retained for the traverses of the flow over the flap made during this test series.

The traversing rig was located at the required chordwise position, wind off, with the direction of traverse normal to the surface. The probe was then positioned well clear of the surface, and once the required flow conditions had been established, was traversed in again towards the surface until contact was indicated by the 'touch-light' system. Pairs of readings of the voltage from the potentiometer, and the pressure at the pitot tube, were taken at this position, and at subsequent positions during the traverse away from the surface, until the pitot pressure became invariant with distance. The spacing used between successive readings depended on the rate of variation of the pitot pressure. A second traverse was then made with the pitot tube replaced by the static tube. The variation of static pressure through the viscous layer was, in general, small, and fewer readings were taken.

The reduction program initially converted the measured pressures into pressure coefficients. A static pressure coefficient, corresponding to the position of each pitot pressure coefficient, was then obtained by linear interpolation from the two adjacent measurements. The ratio of the local velocity to the free-stream velocity, $\dfrac{V}{V_o}$, was subsequently evaluated, as was the ratio $\dfrac{V}{V^*}$, where V^* was the velocity corresponding to the local static pressure coefficient.

This program also performed the integrations to obtain the displacement and momentum thicknesses using linear interpolation between the points on the velocity profile. However, it was found in some of the traverses that the constant value of $\dfrac{V}{V^*}$ reached at the edge of the viscous layer was slightly less than unity. This was attributed to changes in flow direction in the plane of the traverse, which in the region of the slot and shroud trailing edge were large. To correct for this in the evaluation of the displacement and momentum thicknesses a further program was used which adjusted the value of V^* so that it varied linearly across the traverse. At the model surface it was left at its original value but at the outer edge it was changed to give a value of $\dfrac{V}{V^*}$ equal to unity. Typically, this required altering V^* at the outer edge of the profile by about 1 to 3 per cent of its value. Where the wake from the main aerofoil and the flap boundary layer were separate, as was often the case near the slot, the value of V^* in the region of inviscid flow between them was also changed to make $\dfrac{V}{V^*}$ equal to unity, and linear interpolation was again used to obtain V^* across the boundary layer and wake. The program then computed values of the displacement and momentum thicknesses using the corrected velocity profile.

Detailed justification of the above corrections to the velocity profile is not attempted here. However, since the effect of misalignment of a pitot tube with the flow is to produce an apparant loss of pitot pressure, the corrections are in the right direction. The value of the momentum thickness obtained from the corrected velocity profile was, in the most extreme case, 10 per cent less than that obtained using the uncorrected profile, but a more typical difference was 3 per cent. The value of the displacement thickness was less effected.

3.5. *Skin Friction Measurements.*

The skin friction on the model was calculated from the difference between the surface pitot tube pressure and local static pressure, using the calibrations of Quarmby and Das[6], Patel[7] and East[4] for the flattened pitot, circular pitot and razor blade measurements respectively. The limits suggested by Brown and Joubert[8] on the validity of skin friction measurements in pressure gradients were used to check each result. The only measurement which fell outside these limits was obtained very near to the trailing edge for the slatted leading-edge configuration. In this case the skin friction was almost zero.

Before the razor blade technique was used on the model a short experiment was conducted using a flat brass plate in the 4 ft × 3 ft (1·22 m × 0·91 m) wind tunnel at Farnborough, as described in the Appendix. In addition to checking the calibration of the razor blades, the effect of having another blade upstream of the measuring station was determined. It was found that the effect of an upstream blade was negligible provided the separation (in a chordwise direction) was more than about 3 in (8 cm). This enabled simultaneous measurements to be made at a number of chordwise positions along the model surface. In the experiments a spacing of about 6 in (16 cm) was usually employed and further checks showed that, providing they were not in front of or within the transition region, the presence of other blades upstream had no noticeable effect on measurements. If they were ahead of transition the effect on measurements downstream was very obvious and this provided a useful indication of where transition occurred.

The radius of curvature of the model surface was large compared with the razor blade size in all the regions where skin friction was measured. The height of the blade cutting edge above the surface was therefore assumed to be the same as for a flat surface, i.e. half the blade thickness.

4. Discussion of Results.

4.1. Optimum Flap Positions.

4.1.1. Measured values of overall forces.
The overall values of lift coefficient and drag coefficient, for the range of positions and deflections in which the flap was tested, are shown in Figs. 9 to 15. The maximum lift coefficient and drag at a lift coefficient equal to 70 per cent maximum lift coefficient, are summarised in Figs. 16 and 17.

Fig. 9 shows, for the flap deflected 30 degrees, that the maximum lift coefficient is reduced by increasing the overlap of the flap ahead of the shroud trailing edge. The effect of varying the gap between the flap and the wing (measured normal to the chord-line between the flap upper surface and the shroud lower surface) is shown in Fig. 10 for lift, and in Fig. 11 for drag. Over the range of gaps tested, from 0·5 to 4·0 per cent chord, large variations of lift and drag at constant incidence, and of maximum lift, were measured.

As the results for the flap deflected 30 degrees had shown that variation of the gap resulted in much larger changes of lift than variation of overlap, the tests with the flap deflected 10 degrees concentrated on variation of gap. The overlap was 3·1 per cent chord, this being the smallest the flap brackets would allow at this flap deflection. For the plain leading edge, the effect on lift of varying the gap between 1·5 and 2·5 per cent chord is shown in Fig. 12, and on the drag in Fig. 13. The 'peak', occurring in some of the drag curves (Fig. 13), coincides with a change in the form of the pressure distribution on the fairing covering the shroud lower surface, and is associated with changes in the length of the separation bubble which was present on this surface. Figs. 14 and 15 show the effect of variation of the gap, when the plain leading edge had been replaced by the slatted leading edge.

Fig. 16 summarises the effect of gap on the maximum lift coefficient. The experimental technique is least certain here, since with the finite scanning time of the pressure points (up to 35 sec) any transient flow disturbance, of the type which occurs when a wing is close to the stall, will affect a portion of the scan, and thus the total lift. However the results do indicate that for the 30 degree flap deflection the highest value of the maximum lift coefficient occurs with a gap of 2·3 per cent chord. For the range of gaps tested with the flap deflected 10 degrees, and the shroud fairing fitted, the change of maximum lift coefficient with gap was much less than that measured for the same gap range when the flap was deflected 30 degrees. Only three gaps were tested with the plain leading edge, and it is difficult to determine precisely an optimum gap, but both leading-edge configurations tend to indicate an optimum gap at about 2·0 per cent chord. Fig. 17 shows the drag coefficient corresponding to a lift coefficient of 70 per cent maximum lift. The gap for minimum drag would appear to be 2·4 per cent chord for 30 degrees flap deflection, and 2·0 per cent chord for 10 degrees flap deflection—very similar values to those yielding the highest value of the maximum lift coefficient.

4.1.2. Comparison of experimental and theoretical forces.
For the initial assessment of the relative contributions of the mutual interference between the lifting surfaces, and of the viscous flow around the surfaces, the measured variation of the lift on the flap and wing with either incidence or flap position, at the two flap deflections, has been compared with values calculated by the inviscid theory[2]. At this stage, no attempt will be made to analyse the numerical differences which exist between theory and experiment. In order to avoid including in the inviscid calculations the discontinuity in slope which was present for the lower surface of the wing, when tested with 30 degree flap deflection, all the inviscid calculations have assumed the shape of the lower surface of the wing to be as was tested with the flap deflected 10 degrees.

Fig. 18 compares the effect of angle of incidence, for a fixed flap position, at 30 degrees flap deflection. It is noteworthy that, both theoretically and experimentally, the flap lift is almost independent of angle of incidence. The wing lift and the total lift vary in a more conventional manner with angle of incidence, the slopes of the experimental curves being close to those of the theoretical curves.

Fig. 19 compares the effect of overlap of the flap, for a fixed angle of incidence and gap. For the range of positions tested the experimental trends are similar to those predicted by the inviscid calculations. When the inviscid calculations were extended to consider even further aft positions of the flap, it was found that a maximum in the total lift occurred for an overlap of 1 per cent, i.e. when the flap leading edge was just ahead of the shroud trailing edge.

9

Fig. 20 compares the effect of gap, at constant fore-and-aft position and angle of incidence. The measured values of lift now follow the theoretical trend with gap only for values of the gap larger than the optimum. Since, for this flap deflection, there is no optimum in the inviscid results, it can be inferred that the existence of an optimum gap is solely due to the viscous effects. Both the variation of the wing lift with gap, and of the flap lift with gap, depart from the theoretical trends for gaps below the optimum, but the biggest loss of lift occurs for the wing lift. Thus the occurrence of an optimum gap may here be considered as resulting from a change in the effect of the viscous flow on the lift carried by the wing.

The results for the effect of gap at the smaller flap deflection of 10 degrees, with the shroud fairing fitted, shown in Figs. 21 and 22 for the two leading-edge configurations, follow a rather different pattern to that for the 30 degrees flap deflection. The variation of inviscid total lift with gap is very small, but it does have a maximum value at a gap of approximately 2 per cent chord. Both the smallness of the variation of lift, and the position of the highest total lift, are in agreement with the trends found for maximum lift coefficient on Fig. 16. Moreover, the variation of the wing lift and flap lift with gap, for both leading-edge configurations, follow the trends indicated by the inviscid calculations, without the marked departures noted for the 30 degree flap deflection. For this wing and flap configuration, therefore, the optimum gap may be considered as resulting directly from the inviscid effects.

4.1.3. *Deductions from traverses through the viscous layer.* A selection of the results obtained from the traverses through the viscous layers above the flap are shown in Fig. 23, for the 30 degree flap deflection, Fig. 24 for the 10 degree flap deflection with the plain leading edge, and Fig. 25 for the 10 degree flap deflection and the slatted leading edge. The curves show the pitot pressure distribution through the viscous layer, measured normal to the wing or flap surface, but drawn normal to the wing chord for ease of reading. The grid is such that the right-hand ordinate represents full freestream pitot pressure.

With the flap deflected 30 degrees, the traverses of Fig. 23 show that for gaps of 2, 2·5 and 4 per cent chord, freestream pitot pressure was measured at the edge of the flap boundary layer at the shroud trailing-edge position, and that a substantial proportion of this value was measured in the traverses further downstream. In contrast, no such value was measured at the shroud trailing-edge position for the gap of 0·5 per cent chord, and the flow was completely mixed at a very short distance downstream of the shroud trailing edge. For the range of gaps tested with the plain leading edge and the flap deflected 10 degrees, the shroud fairing has resulted in a much reduced boundary-layer thickness on the lower surface of the wing at the shroud trailing edge, so that the flap boundary layer and wing wake are well separated near to the shroud trailing edge (Fig. 24). There is subsequently little interference between the wing wake and the flap boundary layer during the development of the viscous flow over the flap. The one set of traverses made when the slatted leading edge was fitted, Fig. 25, showed that at 2 per cent gap the flap boundary layer and wing wake were again well separated near to the shroud trailing edge, and, even with the thicker wake resulting from the presence of the slat, there is little interference between the development of the wake, and that of the flap boundary layer. Figs. 26 and 27 show that the angle of incidence does not affect the nature of the flow over the flap.

From these traverses, and the force comparisons discussed in 4.1.2, it is possible to suggest a unified explanation for the occurrence of the optimum gaps for the two configurations tested.

For all configurations of wing shroud shape and flap position for which the boundary layer on the flap, and that on the wing shroud, are separated by a region, however small, of freestream pitot pressure, the total lift (and the separate lifts on the wing and flap) will vary with flap position in a manner similar to that predicted by inviscid theory. If the inviscid theory predicts an optimum gap within this range of positions, the experimental optimum will be very close to this value. The limit on this behaviour occurs when the boundary layer on the flap, and that on the shroud lower surface, just meet. Any further reduction of the gap will result in freestream pitot pressure not being reached anywhere in flow through the gap, and the circulation around the wing will be materially reduced because of this. If, therefore, an inviscid optimum does not exist, or exists only for a gap below this value, the optimum gap will be at, or very near to, the smallest gap at which the boundary layer on the flap and shroud are just separate.

These conclusions have a direct implication on the influence of Reynolds number on the optimum gap. For configurations where the optimum gap is defined by the inviscid flow, Reynolds number cannot

affect the optimum gap. For the configurations where the optimum gap is defined by the meeting of the boundary layer on the upper surface of the flap, and the boundary layer on the lower surface of the shroud. Reynolds number will influence the optimum gap. It is to be expected that the optimum gap would decrease with increasing Reynolds number. One series of NACA tests[9], for a wing with a slotted flap deflected 35 degrees, for which the inviscid flow calculations do not show an optimum gap, did suggest a reduction of the optimum gap by about 1 per cent on increasing the Reynolds number from $2\cdot4 \times 10^6$ to $9\cdot0 \times 10^6$.

4.2. *Flap Pressure Distributions and Sectional Shape.*

4.2.1. *Flap pressure distributions.* Fig. 28 shows a typical comparison of the pressure distribution on the flap, when deflected 30 degrees, as measured, and as predicted by inviscid theory. In general the inviscid theory reflects all the features, such as pressure peaks, of the measured pressure distributions, although the peak at the leading edge of the flap is underestimated.

To establish which features of the flap pressure distribution are specific to its position, and which arise from the flap shape, the effect of overlap and gap on the pressure distribution, both from experiment and from theory, are shown in Figs. 29 and 30.

At constant gap, the main effect of changes of the overlap of the flap on the experimental pressure distribution, Fig. 29, is an increase in magnitude of the suction peak at the flap leading edge. The chord-wise position of the second pressure peak, which might perhaps be associated with the presence of the shroud trailing edge, is changed by less than 10 per cent of the movement of the flap. It can therefore be assumed that the existence of the second peak is almost entirely due to the shape of the flap. The corresponding inviscid calculations have overestimated the change of the pressure peak at the flap leading edge. It is possible that this results from the fact that the shape of the shroud lower surface assumed in the inviscid calculations is the same for the two flap positions, whereas the free streamline which this is intended to simulate will probably change its shape when the flap position is changed. The inviscid calculation does, however, reproduce well the effect of fore-and-aft position on the pressure distribution near to the second peak.

The theoretical effect of gap on the pressure distribution, Fig. 30, is modified experimentally by the effects on the circulation of the separation of the flap boundary layer. For the gap of 1 per cent chord, the strong mixing which takes place between the wing wake and the flap boundary layer results in the flow separating at approximately $x_F/c_o = 0\cdot29$ (72 per cent of the flap chord). At a gap of 4 per cent chord, the flap boundary layer and the wing wake are well separated, and there is practically no mixing, but the higher loading associated with this gap results in the boundary layer separating at about the same position as for the 1 per cent gap. For the intermediate gaps the separation point has moved aft to about $x_F/c_o = 0\cdot33$ (82 per cent of the flap chord). Even with these effects, the inviscid pressure distributions do show the salient features of the experimental results; that is a large variation of the suction peak at the flap leading edge with gap, and a more gradual variation of the pressures associated with the second peak. This again indicates that the second peak exists mainly because of the flap shape, with its magnitude having only a small dependence on the flap position.

Figs. 31 and 32 show comparisons between the inviscid and measured pressure distributions on the flap at a deflection of 10 degrees, for the plain leading edge and slatted leading edge respectively. For the range of gaps tested, Figs. 21 and 22 showed that both the inviscid lift and the measured lift change only very slowly with gap, and so these comparisons can be regarded as being typical for this range of gaps. The relationship between the measured and predicted curves are the same for both leading-edge configurations, with a peak in the experimental pressure distribution at $x_F/c_o \simeq 0\cdot06$ which is not predicted by the inviscid theory. The presence of this peak accounts for the closeness of the values of the lift coefficient, as derived from experiment and theory, shown on Figs. 21 and 22. In order to ascertain if this peak was associated with the presence of a separation bubble on the shroud fairing, results have been included on Fig. 32 from tests for which the shroud fairing was removed, so that the wing lower surface was as for the 30 degree flap configuration shown on Fig. 2. It can be seen that the effect on the measured pressure distribution is very small. The peak occurs on the flap at a position just downstream of the shroud trailing

11

edge, and it is therefore considered that this peak arises from the effect of the development of the wake on the flap pressure distribution.

4.2.2. *Effect of flap sectional shape.* In Section 4.2.1. it was shown that the inviscid pressure distribution on the flap at 30 degrees deflection retained the main features of the experimental pressure distribution. Thus a change in the inviscid pressure distribution, resulting from a change of the shape of the flap, should yield a corresponding change in the real flow pressure distribution.

The profile of the lower surface of the flap, and of the upper surface aft of the position of the shroud trailing edge, when the flap is retracted, (in this case at $x_F/c_o = 0.27$) is defined by the basic wing section. The choice of the profile for a further portion of the upper surface is constrained by the shape of the shroud lower surface, this shape itself being determined by structural considerations. Thus the only portion of the contour available for redesign is from $x_F/c_o = 0.05$ on the lower surface to about $x_F/c_o = 0.15$ on the upper surface. However as this region includes both the suction peaks of the measured pressure distributions, it should be possible to modify these peaks by changing the flap contour in this region.

The method of redesign was purely iterative. The pressure distribution at zero angle of incidence and 30 degree flap deflection, with a gap of 2 per cent chord and an overlap of 4.3 per cent chord was taken as the basic configuration. The leading edge of the new flap was defined by a cubic spline curve[10] through three control points at $x_F/c_o = 0.01, 0.06$ and 0.13, to ensure continuity of curvature over the leading edge of the profile. The z coordinates at these control points were varied until the inviscid flow calculation[2] yielded the desired pressure distribution. In this exercise, a roof-top pressure distribution was required, and Fig. 33 compares the original and final pressure distributions on the flap, together with the corresponding leading-edge profiles.

The effect of changes of gap and overlap are shown in Fig. 34. Although the design pressure distribution has no leading-edge suction peak for the design gap of 1.9 per cent chord, the inviscid pressure distributions show that the leading-edge pressure is sensitive to changes of gap and overlap. However the discussion in Section 4.2.1. suggests that the leading-edge suction peak of the corresponding experimental pressure distributions will change less rapidly with gap and overlap than the inviscid calculations would suggest.

It should be noted that as it was assumed not to be possible to alter the flap profile aft of $x_F/c_o = 0.15$, the adverse pressure gradient over the rear of the flap has not been reduced (Fig. 33). Thus any improvement in the lift carried by the new flap, over that carried by the original flap, must result from the improved boundary-layer condition at the beginning of the adverse pressure gradient, resulting from the smoother roof-top pressure distribution. The inviscid pressure distribution on the main wing is virtually unchanged by the substitution of the new flap for the original, and therefore any increase of lift carried by the new flap should be reflected directly in an increase of maximum lift. A flap built to this shape will be tested in the next series of wind-tunnel experiments.

4.3. *Development of the Viscous Layer over the Flap.*

In Section 4.1.3. it was suggested that where inviscid theory does not predict an optimum gap, or where the predicted optimum gap is so small that the wake from the main aerofoil and boundary layer on the flap upper surface would be substantially merged, the optimum in the real flow would occur at a gap where the wake and boundary layer were just separate. It has therefore been considered worthwhile to calculate the development of the boundary layer ignoring the presence of the wake, and *vice-versa*, and to compare the values of the displacement and momentum thicknesses, obtained by adding together the results from the two calculations, with the experimental values for the complete viscous layer (including both wake and boundary layer).

4.3.1. *Boundary layer and wake calculations.* Thwaites' method[11] was used for the laminar boundary-layer calculation. Attempts to predict the position of transition or laminar separation are discussed in Section 4.3.3. The method used for both the turbulent boundary layer and wake calculations was Green's[12] extension of Head's[13] entrainment method. It is primarily intended for compressible flow, but for these calculations the Mach number was taken as zero.

12

The static pressure variation measured on the flap surface was used to calculate the boundary-layer development, and, for the wake, the static pressure along the line of maximum velocity deficit, hereafter called the wake axis, was used. The pressure on the wake axis was determined from the static pressures obtained during traverses through the wake. Since traverses had only been made at a few chordwise positions, curves were drawn of the difference between the static pressure along the wake axis and that on the flap upper surface. These enabled the surface pressure to be 'corrected' to give a more detailed pressure distribution on the wake axis than was directly available from the traverses. A comparison between the pressure on the wake axis and on the flap surface is shown in Fig. 35b.

For the 30 degree flap deflection the calculations were started using the results of traverses through the viscous layer. For the 10 degree flap deflection the wake calculations were started from traverse data but the turbulent boundary-layer calculations were started at the experimentally determined positions of transition, using the value 1·4 for the shape parameter and the value of the momentum thickness predicted by Thwaites' method for the laminar boundary layer. The method described at the end of Section 3.5 was used in the experiments to determine the transition position, except for the case with the slatted leading edge. For the latter case, the momentum thickness of the turbulent boundary layer was extrapolated forward until it equalled the momentum thickness of the laminar boundary layer, so determining the position where transition was assumed to have occurred.

4.3.2. *Comparison with the viscous layer traverses.* Since, in most cases, the wake and boundary layer had merged to a certain extent by the time they reached the trailing edge of the flap it was not always possible to determine the separate boundary layer and wake values of displacement and momentum thickness. However, for the flap deflection of 10 degrees with a gap of 2·5 per cent chord and an angle of incidence of 9 degrees, the wake and boundary layer remained separate, and for this case, therefore, it was possible to compare the wake and boundary-layer developments individually with theory. The results are shown in Fig. 35a. Transition was fixed for this case (as described in Section 2.1.) and, since the thickening effect of the transition strip was unknown, the starting value of the boundary-layer momentum thickness was chosen to give agreement between the calculated value and experiment at the traverse position just downstream of the transition strip. Included in Fig. 35a is the wake calculation by the method of Hill et al[14] where the eddy viscosity has been taken as

$$\varepsilon = 0{\cdot}032 \,.\, V^* \,.\, \theta$$

after Townsend[15]; V^* is evaluated on the wake axis and θ is the wake momentum thickness. Since the entrainment function in Green's wake calculation method[12] is also based on Townsend's data[16] the two methods should, and in fact do, give almost the same wake development. The agreement with experiment in Fig. 35a for both the wake and boundary layer is quite good except very near to the trailing edge where the traverses showed the boundary layer to have separated and, there being no static hole at the trailing edge, the static pressure was not accurately known.

Comparisons between calculated developments of the complete viscous layer are shown for the 30 degree flap deflection in Figs. 36 and 37. The agreement with experiment, although not completely convincing because of the short streamwise extent of the calculation, is fair up to the point of separation of the boundary layer, which was deduced here by examination of the static pressure distribution on the flap surface.

In Figs. 38, 39 and 40 the calculations for the complete viscous layer are compared with experiment for the 10 degree flap deflection. The calculated values of displacement and momentum thickness near to the trailing edge are in fair agreement with experiment except in the case with a slatted leading edge as shown in Fig. 40b. In the latter case the wake velocity profile was substantially different from a Gaussian error function (see Fig. 25) and since the entrainment function for the wake in Green's method is based on the data of Townsend[16], where the velocity profiles were almost exactly Gaussian, some disagreement was to be expected.

4.3.3. *Transition position.* Crabtree's criterion[17] in conjunction with Thwaites' method[11] was used to calculate the position of transition or laminar separation.

For the 30 degree flap deflection, laminar separation was predicted very near to the flap leading edge for gaps of 2·5 and 4 per cent chord, and for a gap of 2 per cent chord the calculated laminar boundary layer became very near to separation there. Since traverses near to the leading edge at $x_F/c_o = 0·03$ gave values of the shape parameter H characteristic of a turbulent boundary layer the experiments and theory were consistent with laminar separation followed by turbulent reattachment between the leading edge and $x_F/c_o = 0·03$.

However, for the 10 degree flap deflection, the experiments disagreed with the Crabtree criterion for transition. In the experiments, the position of transition was determined in the manner described in Section 3.5 and was found to vary between $x_F/c_o = 0·08$ and $x_F/c_o = 0·17$, depending on the experimental conditions. The transition position in each case is indicated in Figs. 38, 39 and 40. In the theory, transition was not predicted, but the laminar boundary-layer calculation was terminated by laminar separation in the region $0·20 < x_F/c_o < 0·25$ for all the results for 10 degree flap deflection.

The fact that the Crabtree criterion failed to predict transition was attributed to disturbances produced by the turbulent wake over the flap. Irrotational fluctuations in velocity occur outside the turbulent core of a wake (*see*, for example, Ref. 16) and these might be expected to have a similar effect to that of a high level of freestream turbulence, in which Crabtree's criterion was not intended to be applicable. It is thus possible to envisage transition occurring somewhat upstream of the point where the turbulent core of the wake encroached on the boundary layer, provided of course that the boundary layer was not already turbulent and that the laminar boundary layer had developed beyond the conditions for Tollmien-Schlichting instability[18]. In all the results for 10 degree flap deflection, calculations of the position for the onset of Tollmien-Schlichting instability, using the method described by Schlichting[18], showed that it occurred at $x_F/c_o = 0·06$ approximately. The experimentally determined positions of transition (between $x_F/c_o = 0·08$ and $x_F/c_o = 0·17$) were therefore all in the region where the laminar boundary layer was unstable to disturbances from the wake.

4.3.4. *Skin friction development and separation.* The calculated skin friction is compared with experimental results for the 30 degree flap deflection in Figs. 41 and 42. Owing to the thinness of the boundary layer near the leading edge the starting values of shape parameter and momentum thickness were not of high accuracy and the calculation was therefore also carried out starting from traverse data at $x_F/c_o = 0·114$, as a check on the effect of this on the calculation. Near to the trailing edge it can be seen that there is little difference in results using the two starting positions.

The agreement with experiment was worst for a gap of 4 per cent chord, which was not expected since there was least interference by the wake for this condition. However, there was fair agreement for the other gaps. The points of separation shown in Figs. 41 and 42 were deduced by examination of the measured pressure distribution on the flap. The calculation method, when using the measured pressure distributions, does not predict separation, but if the calculated skin friction is ignored in that region and instead extrapolated to zero, the point of zero skin friction in the four cases is not far downstream of the separation point deduced from the pressure distributions.

The results of the skin friction calculations for the 10 degree flap deflection are shown in Figs. 43, 44 and 45. The closeness to the measured skin friction was similar to that for the 30 degree flap deflection.

From the above skin friction calculations, it can be concluded that neglecting the effect of the wake on the turbulent boundary layer entirely does not lead to large errors for flap gaps near to the optimum. In view of the lack, at present, of a method of accounting for the interaction of the wake with the boundary layer this is a helpful simplification.

5. *Conclusions and Future Work.*

It is now possible to summarise the details of the flow around the slotted flap, and to suggest how this research work might be extended.

It has been shown that, when the flap position for optimum lift is being sought, the choice of the gap is more critical than that of the overlap. This flap position is influenced by both the inviscid solution, and

14

the viscous interaction, the relative contributions being dependant on the form of the inviscid solution. It has been suggested that Reynolds number can, in some circumstances, influence the value of the optimum gap· with the optimum gap decreasing with increasing Reynolds number. As, at this optimum gap, the boundary layers on the shroud lower surface and flap upper surface just meet, it should be possible to predict the effect of Reynolds number on optimum gap.

The lift of the wing and flap combination, as well as the optimum position of the flap, is determined by the inviscid flow pressure distributions, together with the effects of the developments of the boundary layers and wakes. In any prediction method, therefore, all these contributions must be estimated with sufficient accuracy.

It is considered that the accuracy of the method of calculating the inviscid pressure distribution is sufficient for any prediction method, although confirmation of this, by the use of an exact test case for a multiple aerofoil, would be of advantage. Near to the optimum flap position, it has been shown that there is only weak interference between the flap boundary layer and the wing wake. Thus the measured boundary layer and wake parameters, and the surface skin friction, can probably be predicted with sufficient accuracy by existing calculation methods, in which the interference has been completely ignored. To determine the optimum configuration, and for off-design conditions, interference can probably not be ignored and a calculation method is needed for the simultaneous development of the wake and the boundary layer. This constitutes one area of future research. It has not yet been possible to estimate the influence of the wake from the wing on the lift of the flap. It may be that this effect is small, and thus the estimation method need not be of high accuracy. Nevertheless this contribution is important, and this is a second area of future research.

Whilst, therefore, a complete design and analysis method has not been presented at this time, it is considered that the results given in this Report show that the flow over a slotted flap is relatively simple, and that the situation should be capable of yielding the desired design and analysis method without great extensions of present knowledge. How these concepts apply to a flap on a sweptback wing remains to be determined, and will be the subject of future wind-tunnel experiments.

15

LIST OF SYMBOLS

c_o	Chord of wing with high-lift devices retracted
C_D	Drag coefficient
C_{f_o}	Skin friction coefficient, based on freestream conditions
C_L	Lift coefficient
$C_{L_{max}}$	Maximum lift coefficient
C_p	Pressure coefficient
C_{pH}	Pressure coefficient corresponding to pitot pressure at wake rake
C_{ps}	Pressure coefficient corresponding to static pressure at wake rake
C_σ	Suction flow coefficient $= \dfrac{m}{2\rho\, V_o\, \delta_t^*\, t}$
h	Height of razor blade from wing surface to cutting edge
H	Boundary-layer shape parameter $= \delta^*/\theta$
m	Suction mass flow rate (both ends of model)
Δp	Pressure measured by razor blade minus local static pressure (razor blade removed)
p_o	Static pressure in freestream
p_H	Pitot pressure
q_o	Freestream dynamic pressure
t	Maximum wing thickness
V	Local velocity in boundary layer
V_o	Freestream velocity
V^*	Velocity corresponding to local static pressure coefficient
x	Distance parallel to aerofoil component chord-line, measured from component leading edge
x_F	Distance along flap chord, measured from flap leading edge
x_W	Distance along wing chord, measured from wing leading edge
x^*	Defined as $\log_{10}\left\{\dfrac{\Delta p\, h^2}{\rho\, v^2}\right\}$

y^* Defined as $\log_{10}\left\{\dfrac{\tau\,h^2}{\rho\,v^2}\right\}$

z_B Distance normal to flap surface, measured from flap surface

z_W Distance across wake

z Distance normal to aerofoil component chord, measured from component chord-line

α Angle of incidence

δ^* Boundary-layer displacement thickness

δ_t^* Displacement thickness of boundary layer on wall of wind tunnel, measured at the position of the model, tunnel empty

ε Eddy viscosity

θ Boundary-layer momentum thickness

ρ Fluid density

τ Skin friction

v Kinematic viscosity of fluid

REFERENCES

No.	Author(s)	Title, etc.
1	A. D. Young	The aerodynamic characteristics of flaps. A.R.C. 10766, R. & M. 2622 (1947).
2	A. M. O. Smith and J. L. Hess	Calculation of potential flow about arbitrary bodies. Progress in Aeronautical Sciences, Vol. 8, Pergamon Press, London (1966).
3	D. N. Foster and J. A. Lawford	Experimental attempts to obtain uniform loading over two-dimensional high-lift wings. R.A.E. Technical Report 68283 (A.R.C. 31098) (1968).
4	L. F. East	Measurement of skin friction at low subsonic speeds by the razor blade technique. A.R.C. R. & M. 3525 (1966).
5	B. Melvill Jones	Measurement of profile drag by the pitot-traverse method. A.R.C. R. & M. 1688 (1936).
6	A. Quarmby and H. K. Das	Measurement of skin friction using a rectangular mouthed Preston tube. Aeronautical Journal, Vol. 73, No. 699 (1969).
7	V. C. Patel	Calibration of the Preston tube and limitations on its use in pressure gradients. J. Fluid Mech., Vol. 23, Part 1 (1965).
8	K. C. Brown and P. N. Joubert	The measurement of skin friction in turbulent boundary layers with adverse pressure gradients. J. Fluid. Mech., Vol. 35, Part 4 (1969).
9	S. F. Racisz	Investigation of NACA 65 (112) A111 (approx.) airfoil with 0·35 chord slotted flap at Reynolds numbers up to 25 million. NACA TN 1463 (1947).
10	J. M. Freeland	Cubic spline fitting. R.A.E. Maths Computing Notes Series C 335 (1965).
11	B. Thwaites	Incompressible aerodynamics. Fluid motion memoirs. Clarendon Press (1960).
12	J. E. Green	Head's method in compressible flow. to be published.
13	M. R. Head	Entrainment in the turbulent boundary layer. A.R.C. R. & M. 3152 (1958).
14	P. G. Hill, U. W. Schaub and Y. Senoo	Turbulent wakes in pressure gradients. Transactions of the A.S.M.E., 63–WA5 (1963).

REFERENCES—*continued*

15   A. A. Townsend   ..   ..   Structure of turbulent shear flow.
                                   Cambridge University Press (1956).

16   A. A. Townsend   ..   ..   The mechanism of entrainment in free turbulent flows.
                                   J. Fluid. Mech., Vol. 26, Part 4 (1966).

17   L. F. Crabtree   ..   ..   Prediction of transition in the boundary layer on an aerofoil.
                                   A.R.C. 19310 (1957).

18   H. Schlichting   ..   ..   Boundary layer theory.
                                   Fourth edition, pp. 414, McGraw-Hill (1960).

APPENDIX

The Application of the Razor Blade Technique
for the Measurement of Skin Friction

It was important that the method chosen to hold the razor blades in position on the model should enable them to be quickly put on and removed, without damaging the surface, and to be held firmly enough to prevent their moving during the measurements. The method adopted was to fasten a small piece of sellotape over each end of the blade, as shown in Fig. 7. This left the centre section of the blade free from the additional thickness of the sellotape, which could effect the calibration.

The check experiment in the 4 ft $\times$ 3 ft (1·22m $\times$ 0·91m) wind tunnel compared results obtained using razor blades attached to a brass plate, with skin friction values derived from measurements using circular pitot tubes and Patel's calibration. Brass was not found to be a good surface for the sellotape to adhere to, and this caused some scatter in the results. However, the results agreed sufficiently well with East's calibration[4] for razor blades (Fig. 7) for that calibration to be used in the main experiments. Moreover, the model surface of glass reinforced plastic afforded a better grip for the sellotape, and repeated measurements were in good agreement with each other.

TABLE 1

Coordinates of Components of Wing Section

Main wing

(a) Leading edge drooped 10 degrees, no shroud fairing.

Upper surface			Lower surface	
x/c	z/c_o		x/c_o	z/c_o
-0.00599	-0.02224		-0.00587	-0.02786
-0.00398	-0.01758		-0.00422	-0.03142
-0.00157	-0.01385		-0.00038	-0.03483
0.00216	-0.00959		0.00412	-0.03722
0.00599	-0.00608		0.00886	-0.03901
0.00972	-0.00307		0.01340	-0.04019
0.01883	0.00307		0.01842	-0.04129
0.02793	0.00881		0.02708	-0.04278
0.03716	0.01385		0.03746	-0.04418
0.05585	0.02319		0.04809	-0.04532
0.07469	0.03175		0.08880	-0.04789
0.09357	0.03933		0.12982	-0.04882
0.11270	0.04635		0.16995	-0.05201
0.12120	0.04911		0.21000	-0.05742
0.12984	0.05000		0.24986	-0.06182
0.14010	0.05324		0.28986	-0.06486
0.15018	0.05483		0.32970	-0.06683
0.17023	0.05775		0.36992	-0.06774
0.19024	0.06036		0.40998	-0.06756
0.21027	0.06261		0.45026	-0.06586
0.25023	0.06647		0.49016	-0.06251
0.29027	0.06924		0.53029	-0.05835
0.32980	0.07113		0.57151	-0.05304
0.37006	0.07203		0.59296	-0.05028
0.40973	0.07201		0.60978	-0.02750
0.44982	0.07128		0.62852	-0.01071
0.48983	0.06958		0.65868	0.00478
0.52995	0.06743		0.69150	0.01482
0.56924	0.06439		0.72402	0.02117
0.62706	0.05922		0.75070	0.02429
0.69015	0.05229		0.79118	0.02597
0.74952	0.04439		0.82601	0.02561
0.78939	0.03857		0.85978	0.02388
0.82473	0.03325		0.87004	0.02304
0.85820	0.02783			
0.87004	0.02582			

TABLE 1—*continued*

(b) Plain leading edge with shroud fairing.

Upper surface		Lower surface	
x/c_o	z/c_o	x/c_o	z/c_o
0·00000	0·00000	0·00000	0·00000
0·00104	0·00417	0·00113	−0·00486
0·00380	0·00850	0·00434	−0·00917
0·00691	0·01186	0·00822	−0·01203
0·01134	0·01550	0·01251	−0·01451
0·01564	0·01819	0·01686	−0·01650
0·01976	0·02053	0·02148	−0·01846
0·02991	0·02525	0·02997	−0·02144
0·03987	0·02925	0·03983	−0·02458
0·04985	0·03275	0·05025	−0·02761
0·06988	0·03851	0·08982	−0·03722
0·08989	0·04356	0·13013	−0·04519
0·10984	0·04786	0·16995	−0·05201
0·12986	0·05139	0·21000	−0·05742
0·14001	0·05317	0·24986	−0·06182
0·15020	0·05486	0·28986	−0·06486
0·17015	0·05785	0·32970	−0·06683
0·19013	0·06033	0·36992	−0·06774
0·21028	0·06264	0·40998	−0·06756
0·25023	0·06647	0·45026	−0·06586
0·29027	0·06924	0·49016	−0·06251
0·32980	0·07113	0·53029	−0·05835
0·37006	0·07203	0·57151	−0·05304
0·40973	0·07201	0·59361	−0·05031
0·44982	0·07128	0·62000	−0·04717
0·48983	0·06958	0·64479	−0·04289
0·52995	0·06743	0·66986	−0·03756
0·56924	0·06439	0·70537	−0·02669
0·62706	0·05922	0·73046	−0·01486
0·69015	0·05229	0·75783	0·00142
0·74952	0·04439	0·78043	0·01561
0·78939	0·03857	0·80635	0·02542
0·82473	0·03325	0·82581	0·02556
0·85820	0·02783	0·85978	0·02388
0·87004	0·02582	0·87004	0·02304

TABLE 1—*continued*

(c) Slatted leading edge. (Slat partition line.)

Upper surface	
x/c_o	z/c_o
0·03997	−0·01583
0·04109	−0·00894
0·04339	−0·00355
0·04761	0·00153
0·05445	0·00769
0·06104	0·01264
0·06994	0·01797
0·08049	0·02361
0·09461	0·03064
0·10915	0·03644
0·12416	0·04186
0·14030	0·04717
0·15423	0·05144
0·16975	0·05556
0·18466	0·05856
0·21977	0·06367

Lower surface	
x/c_o	z/c_o
0·04096	−0·02292
0·04764	−0·02675
0·05450	−0·02858
0·06993	−0·03250
0·09458	−0·03836
0·14046	−0·04703
0·18433	−0·05386

Flap

Upper surface	
x_F/c_o	z_F/c_o
0·00000	− 0·04147
0·00265	− 0·03517
0·01020	− 0·02561
0·01794	− 0·01747
0·02780	− 0·00922
0·03764	− 0·00275
0·04843	0·00258
0·05935	0·00661
0·07115	0·00958
0·08393	0·01197
0·09492	0·01392
0·11378	0·01675
0·13926	0·02006
0·17027	0·02264
0·20413	0·02381
0·24172	0·02303
0·28080	0·02039
0·31579	0·01644
0·35536	0·00986
0·37640	0·00553
0·39053	0·00242
0·40000	0·00000

Lower surface	
x_F/c_o	z_F/c_o
0·00287	− 0·04655
0·00954	− 0·04778
0·03199	− 0·04447
0·05701	− 0·04094
0·08426	− 0·03686
0·11373	− 0·03261
0·14616	− 0·02803
0·19625	− 0·02161
0·24192	− 0·01528
0·29008	− 0·00967
0·33604	− 0·00494
0·36932	− 0·00211
0·38828	− 0·00010
0·40000	0·00000

24

FIG. 1. Model in wind tunnel.

Plain leading edge; flap deflected 10°

10°

Hinge point, 0·15C₀

Leading edge deflected 10°; flap deflected 30°

0·87C₀

0·17C₀

0·40C₀

Slatted leading edge; slat deflected 28°; flap deflected 10°
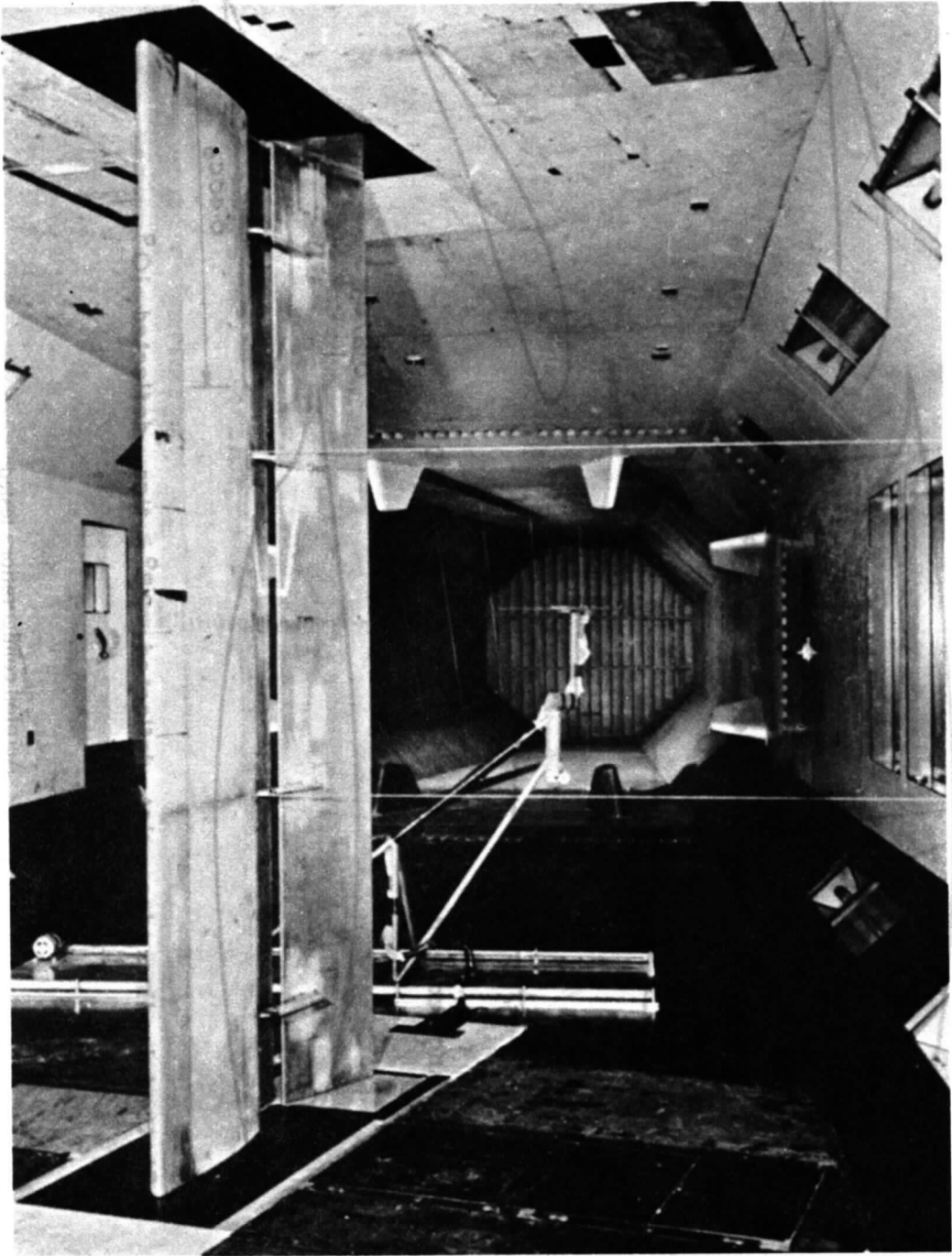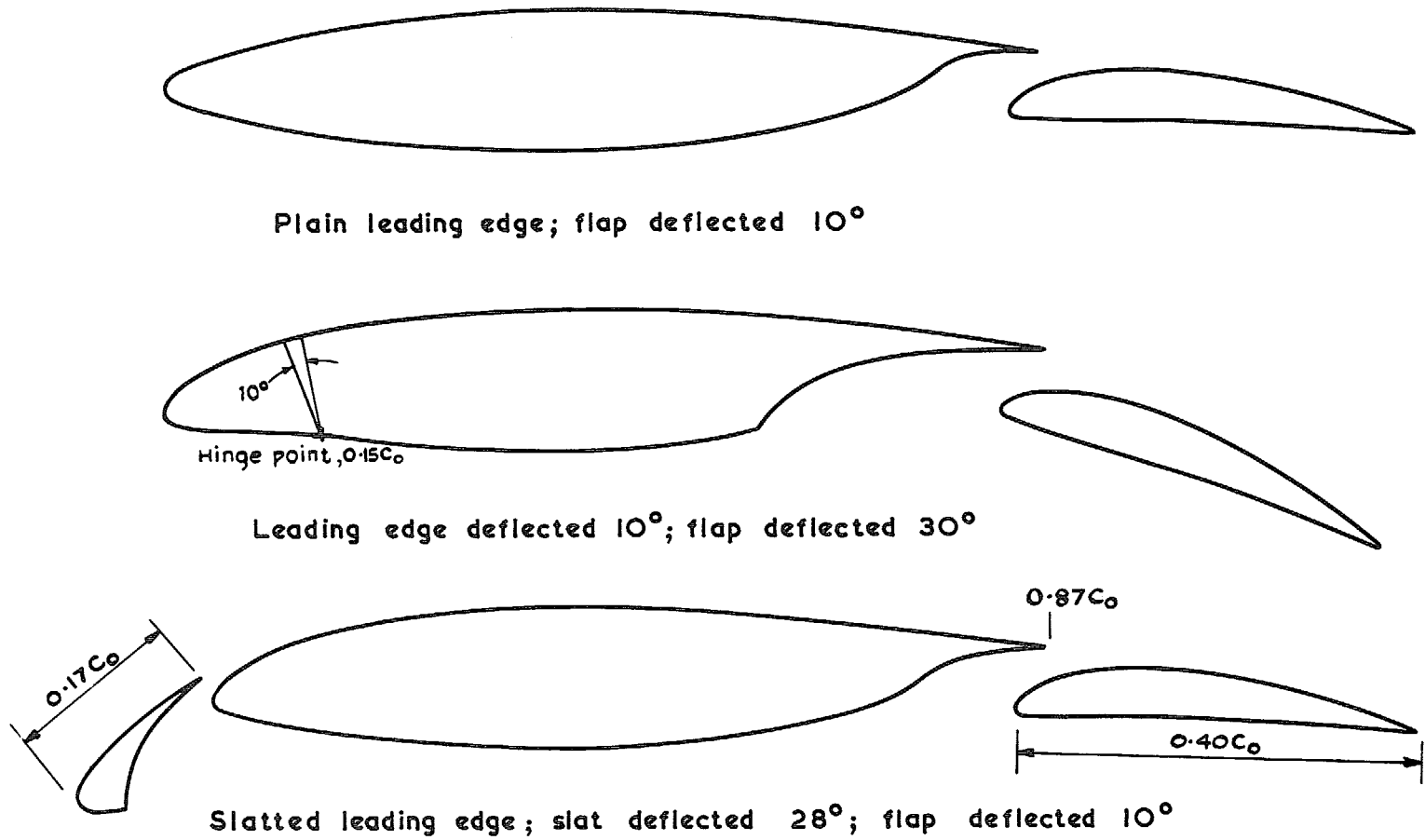
FIG. 2. Aerofoil configurations tested.

26

Plan

20 ft (6·10 m) to end of contraction

21·5 ft (6·55 m) to beginning of first diffuser

13ft (3·96m)

Track of wake survey rake

Straining wires

Strain-gauged link

Elevation

Roof

Pressure tapping section on tunnel centre line

9ft (2·74m)

Pivot and actuator for rotation of rake

Carriage for lateral movement

Floor

Pivots of straining wires
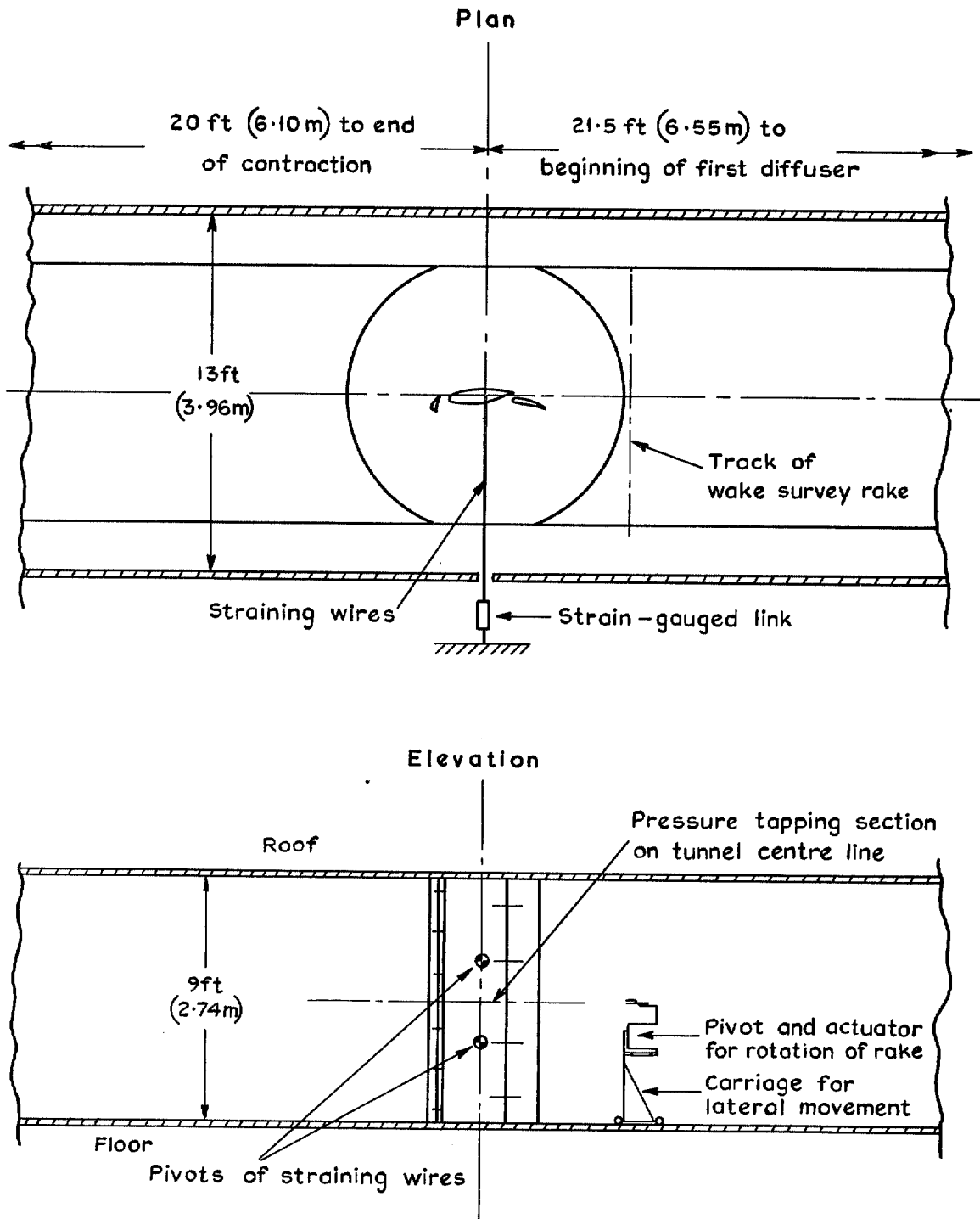
FIG. 3.   Mounting of model in wind tunnel (diagrammatic). Wall-suction details omitted for clarity.

A A

Movement
normal to
chord line

Locking
wedge

Screw
adjustment

Section A A

Locking
wedge

Screw
adjustment

Movement parallel
to chord line

Bracket
carrying flap
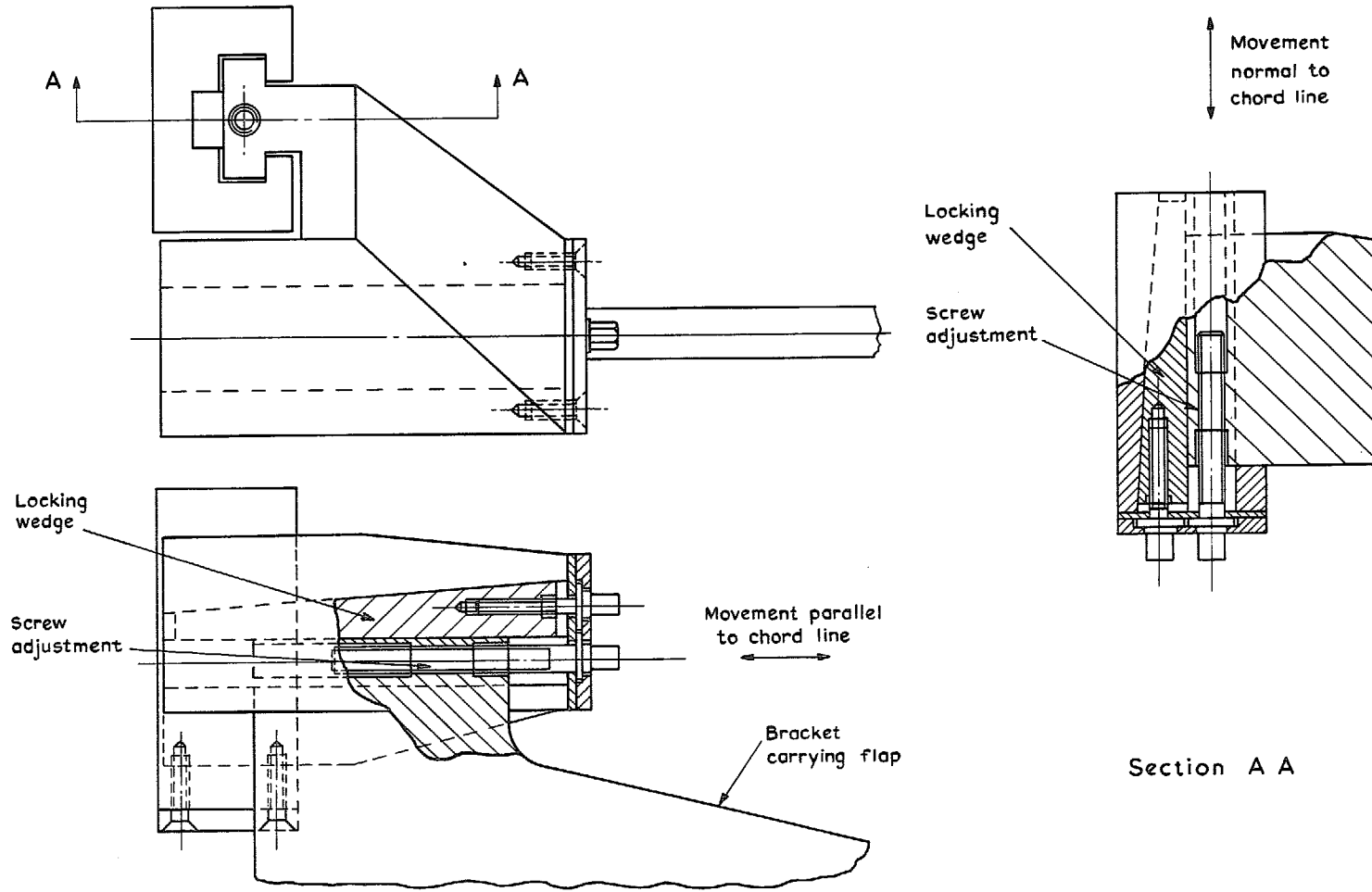
FIG. 4.   Details of jacking mechanism for positioning the flap.

Plan

Perforated surfaces

0·17in diam holes at
0·50in pitch 0·25in
from model

18·6in
(47·4 cm)

51·5in (131cm)

Elevation

Support webs

5in
(12·7cm)

Suction
-delivery pipes

Suction manifold
to pump

Details of
support for
perforated surfaces

Perforated sheet

Lattice of
thin plates

Thick base
plate with
1in dia holes
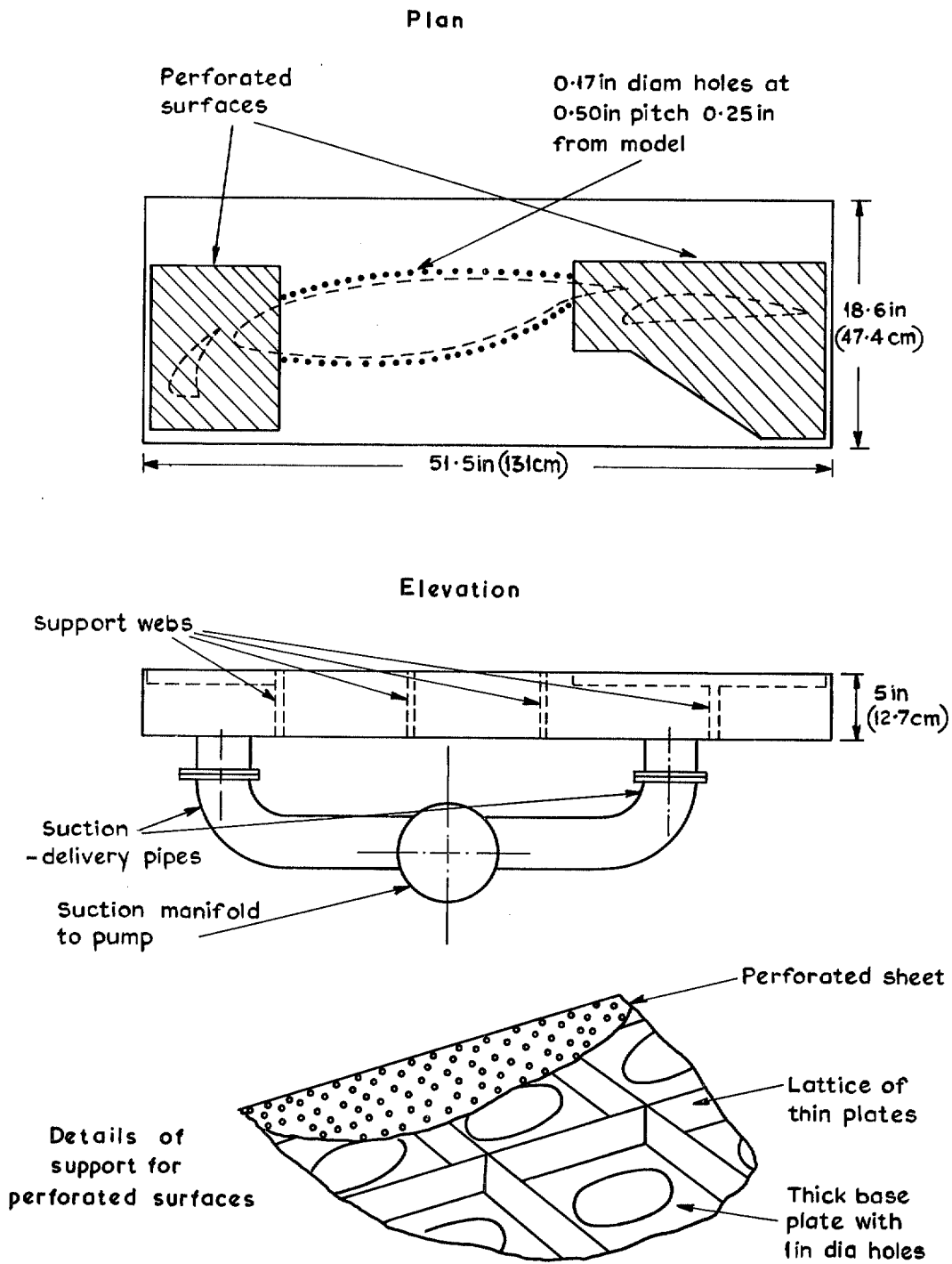
Fig. 5.   Details of suction boxes.

Linear potentiometer

Spring-loaded spindle

0·008 in (0·20mm)

0·0025 in (0·06mm)

0·003 in (·08mm)

0·0195 in (0·50mm)

·0105 in (0·27mm)

Rectangular pitot-tube   Round pitot-tube

6·65 cm (16·9 cm)

Electrical leads for potentiometer

1·25 in (3·18 cm)

9·85 in (25·0 cm)

0·117 in diam (3·0 mm)

0·080 in diam (2·0 mm)

1·25 in (3·18 cm)

Stiffening web

Hydraulic oil pipes

Electrical lead for touchdown detection system

Jack maximum extension 4·00 in (10·4 cm)

Square double acting jack

To pressure measuring system

FIG. 6.   Remotely controlled traversing mechanism, and pitot tubes.

30

0·26 in
(0·66 cm)

Selloptape

Razor blade

Position of static hole

0·74 in (1·88 cm)

h

Static hole

0·0100 in ±·0002
(0·254 mm)

$5\frac{1}{4}^{\circ}$

0·0148 in
(0·376 mm)
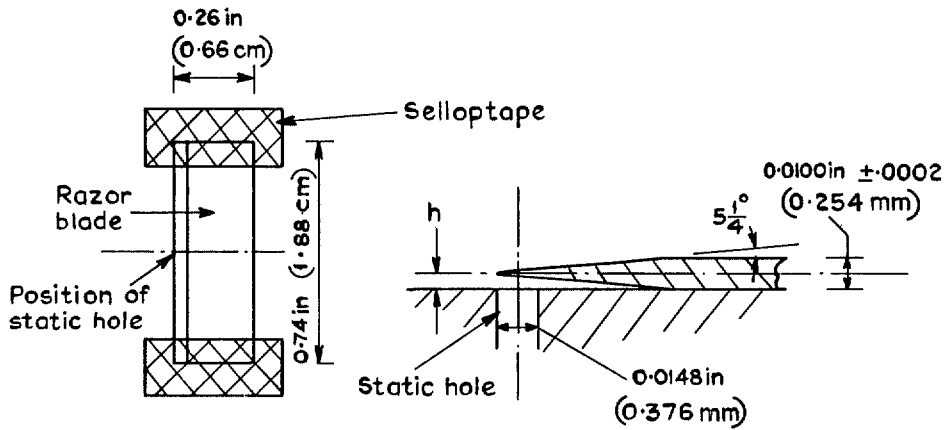
Use of razor blade for measurement of skin friction

$y^* = Log_{10}\left(\dfrac{\tau h^2}{\rho v^2}\right)$

$x^* = log_{10}\left(\dfrac{\Delta p h^2}{\rho v^2}\right)$

East's calibration (Ref 4)
$y^* = -0·23 + 0·618 x^* + 0·0165 x^{*2}$

Spread of experimental results
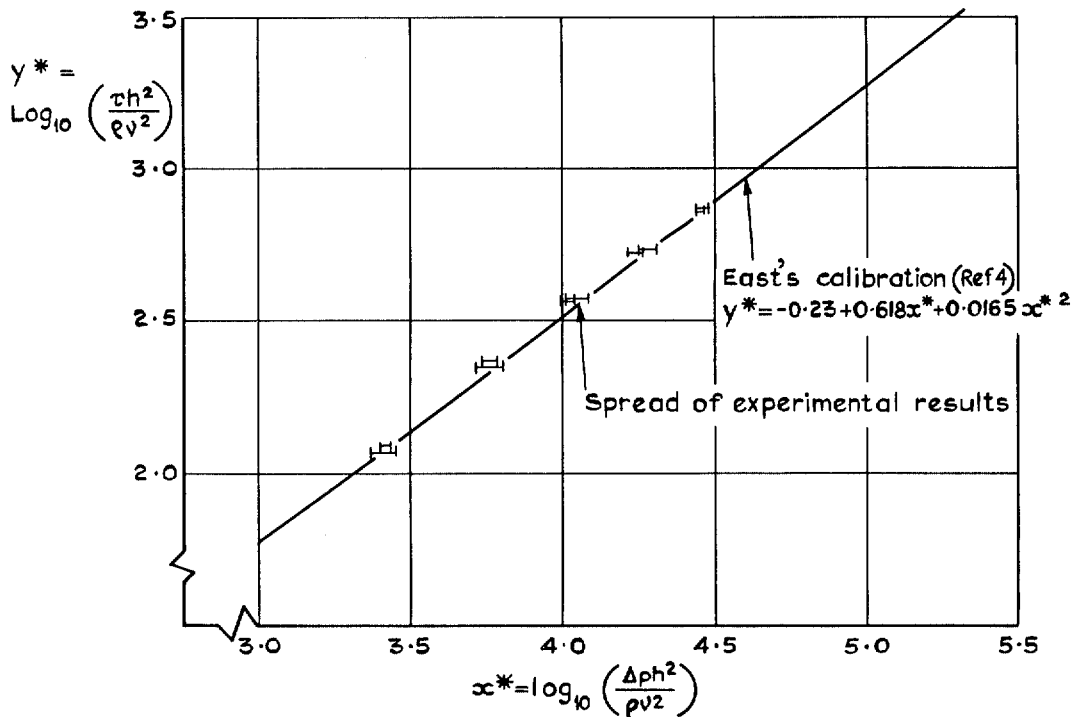
Calibration of razor blades held on by sellotape

FIG. 7.   Method of use, and calibration, of razor blades.
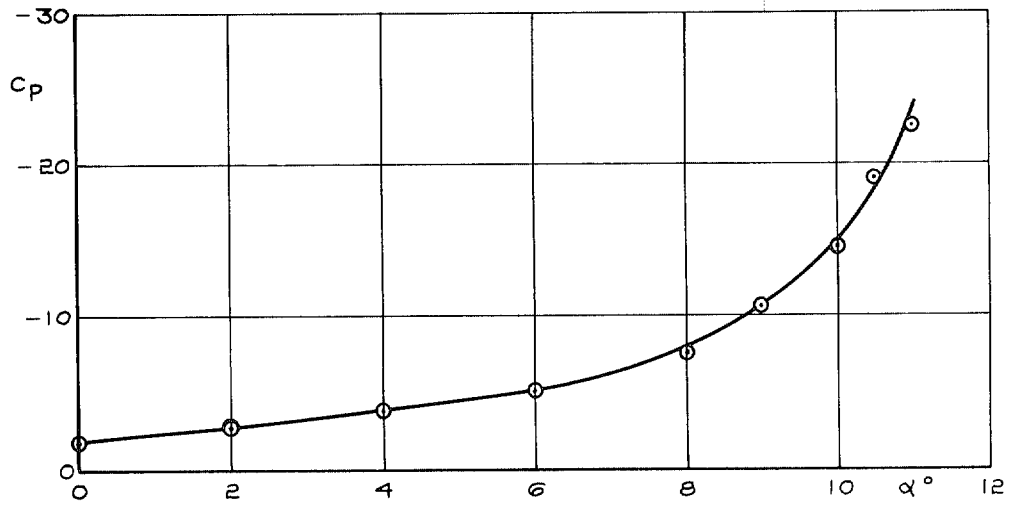
a   Suction pressures
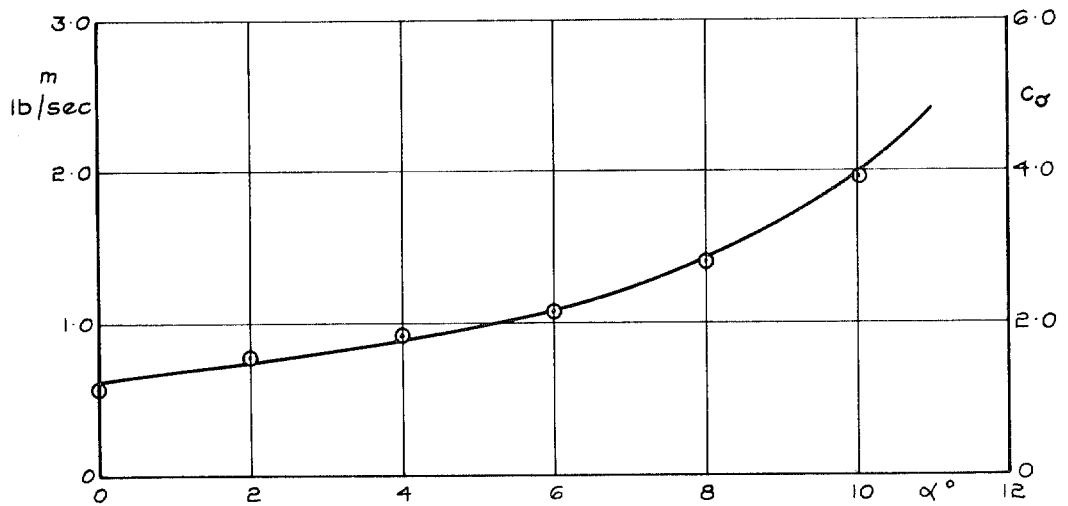
b   Suction quantities

FIG. 8. a. & b.   Pressures and flow quantities for wall boundary-layer control system. Flap deflection 30°
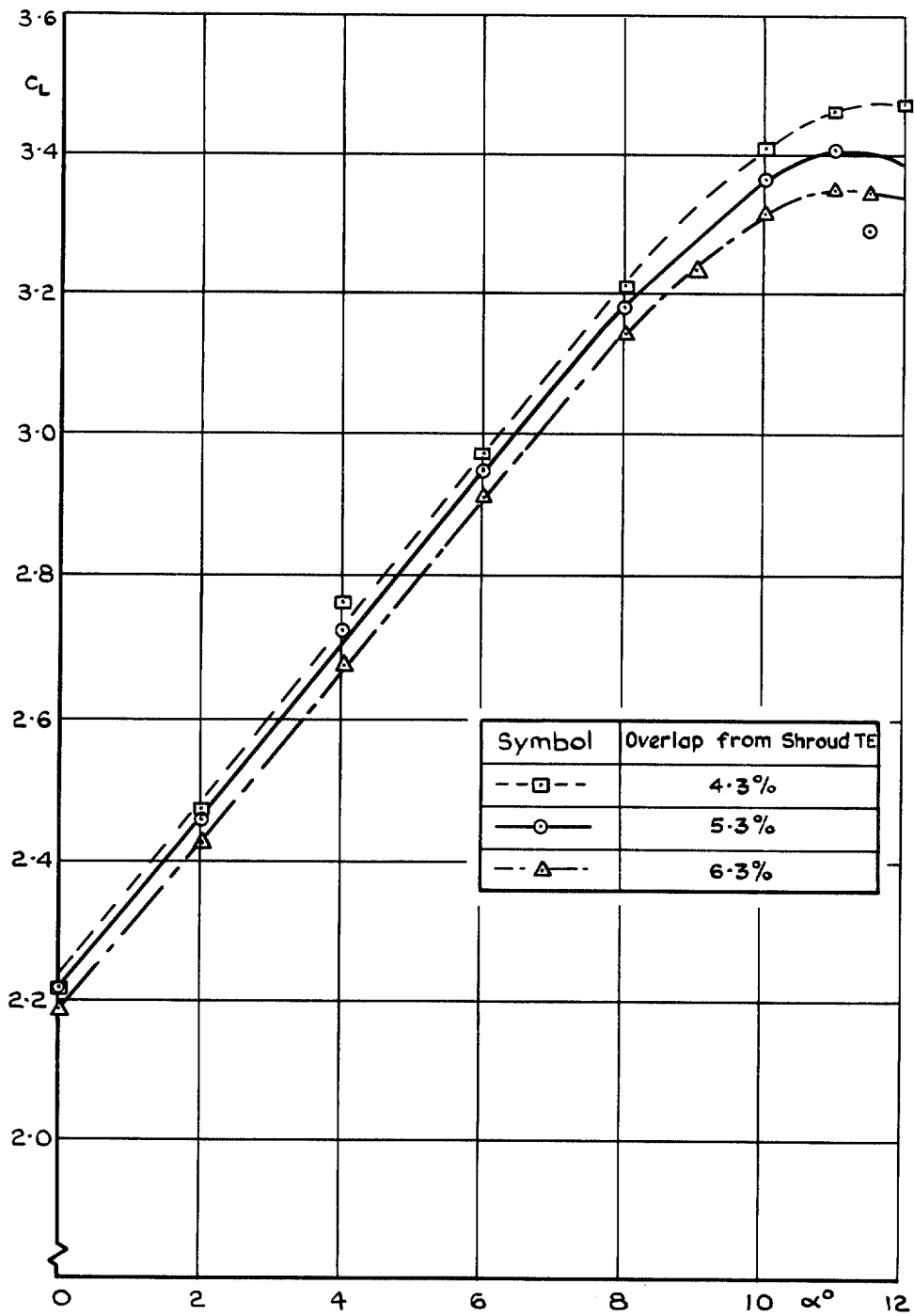
FIG. 9.   Effect of overlap from shroud trailing edge. Flap deflection 30°.
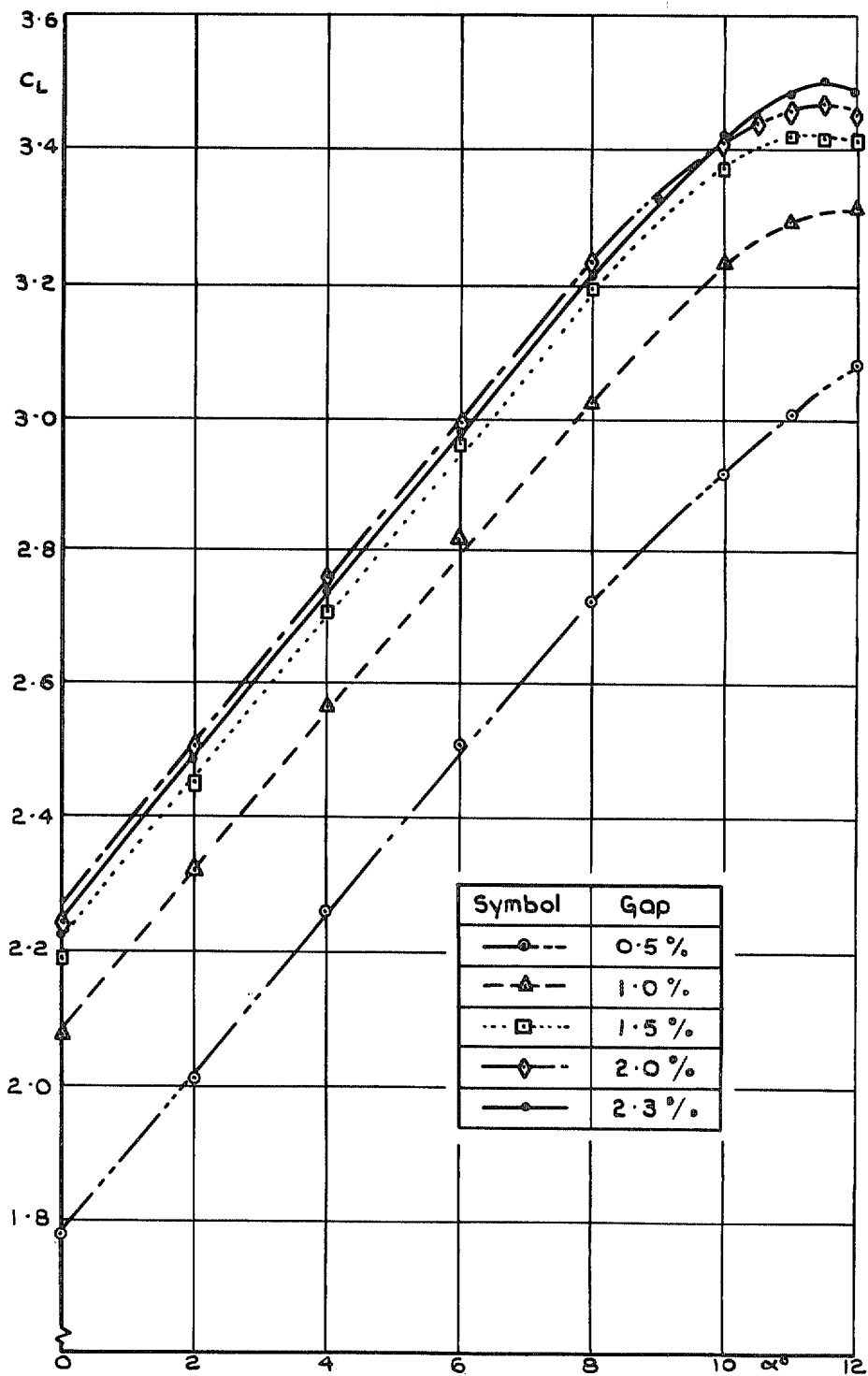
FIG. 10a.   Effect of gap on lift. Gap $\leqslant$ 2·3%, Flap deflection 30°.

34
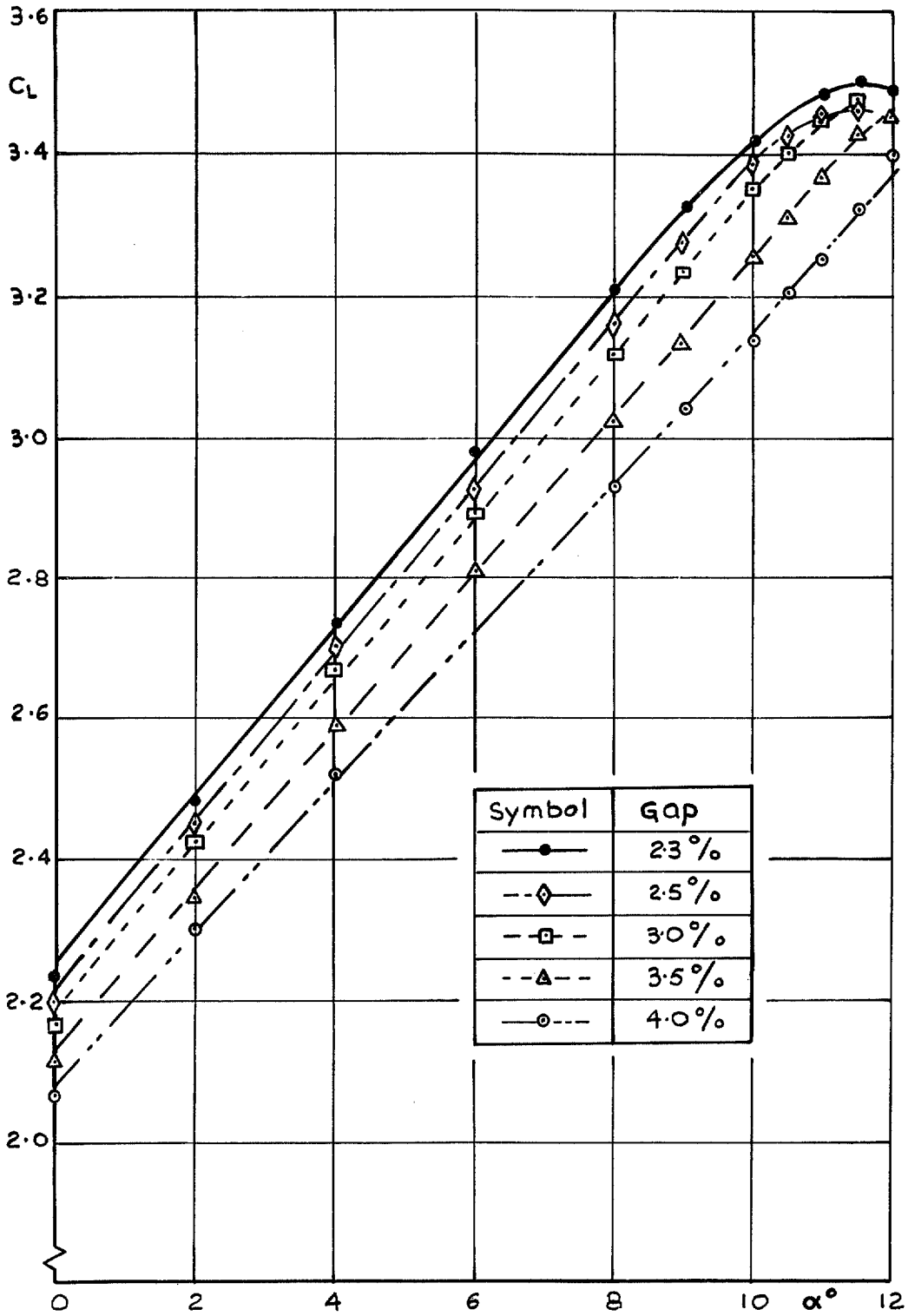
FIG. 10b.   Effect of gap on lift. Gap $\geqslant 2 \cdot 3\%$, Flap deflection 30°.

35
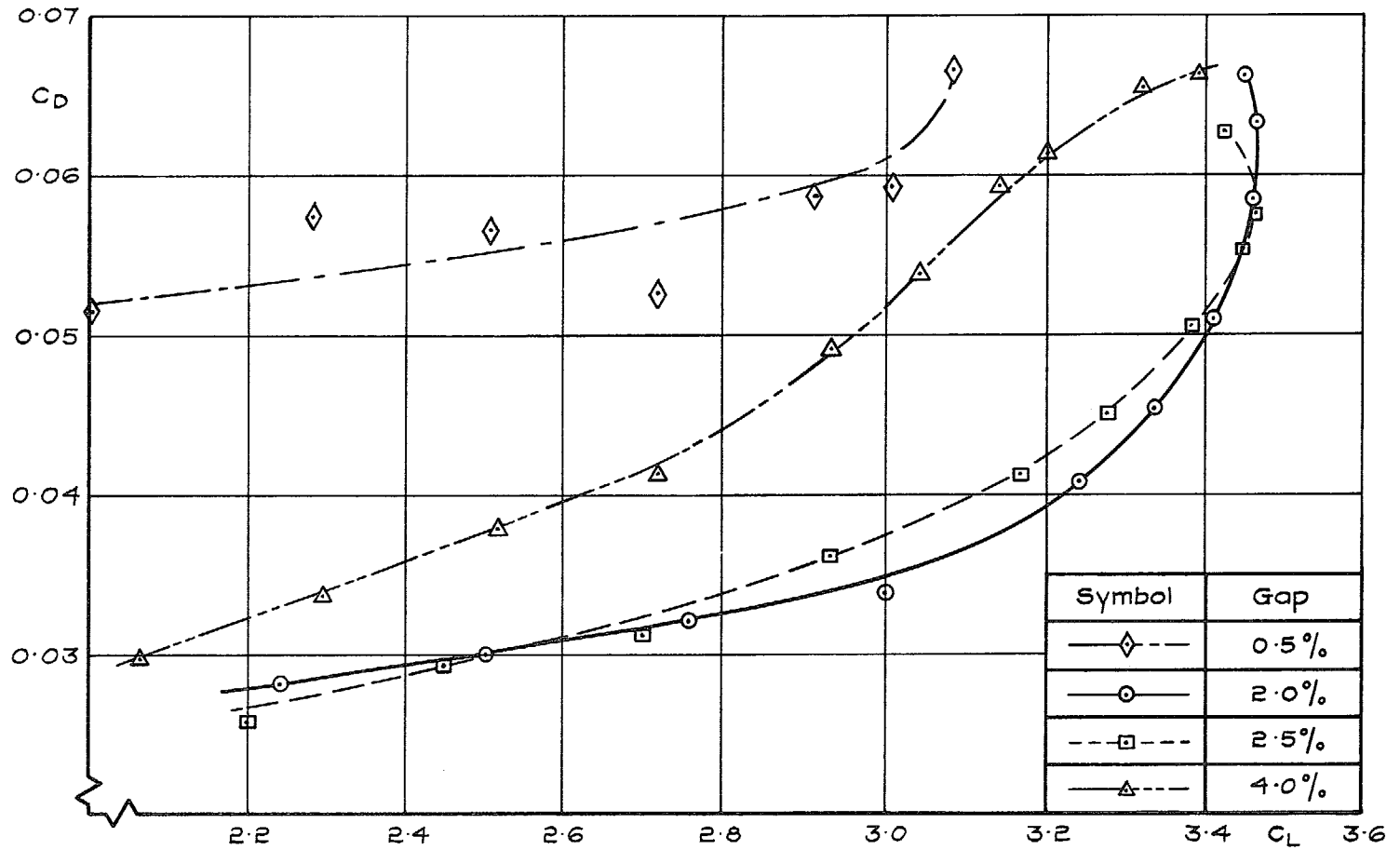
Fig. 11. Variation of sectional drag with lift and gap. Flap deflection 30°.
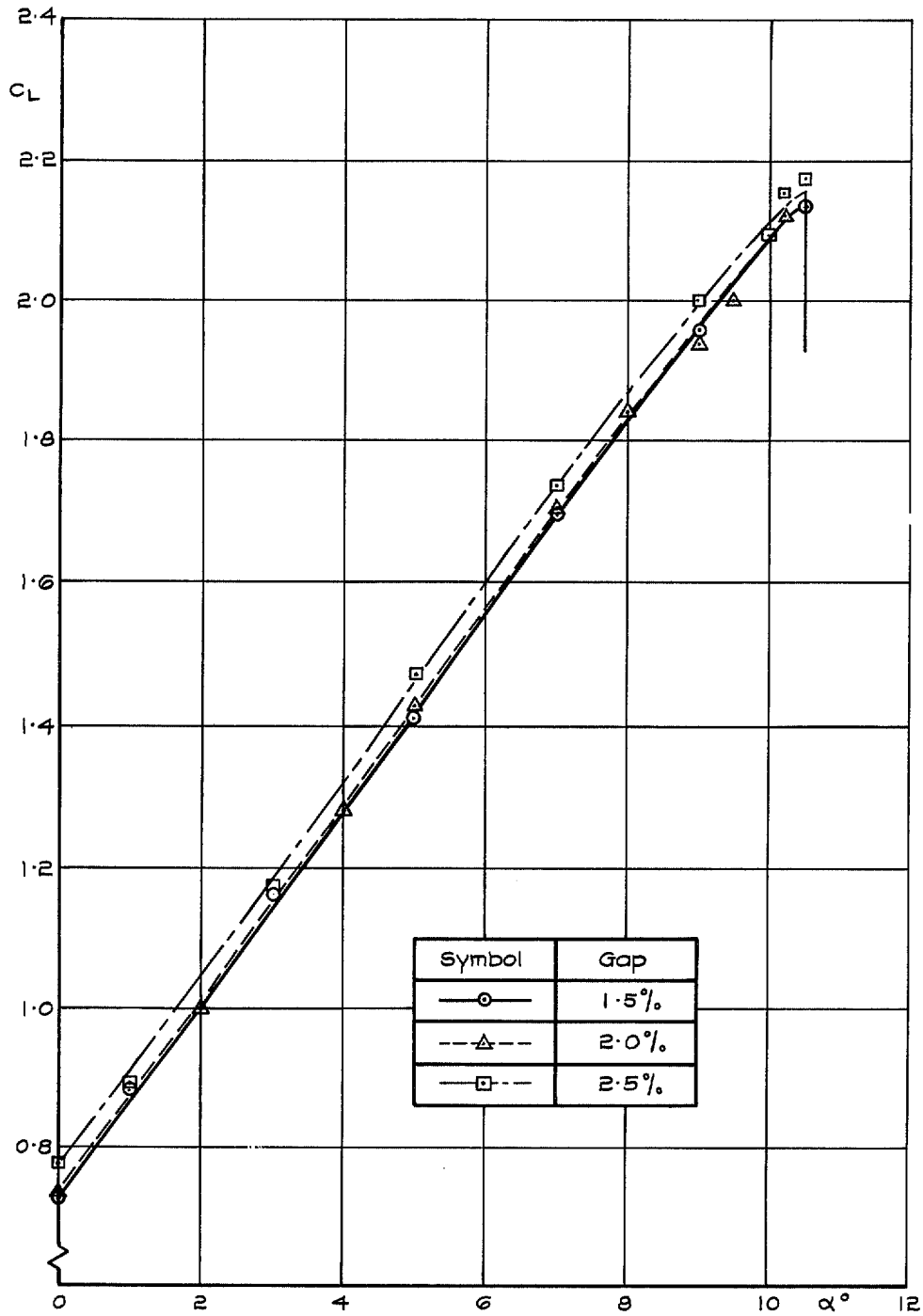
FIG. 12. Effect of gap on lift. Flap deflection 10°, plain leading edge.
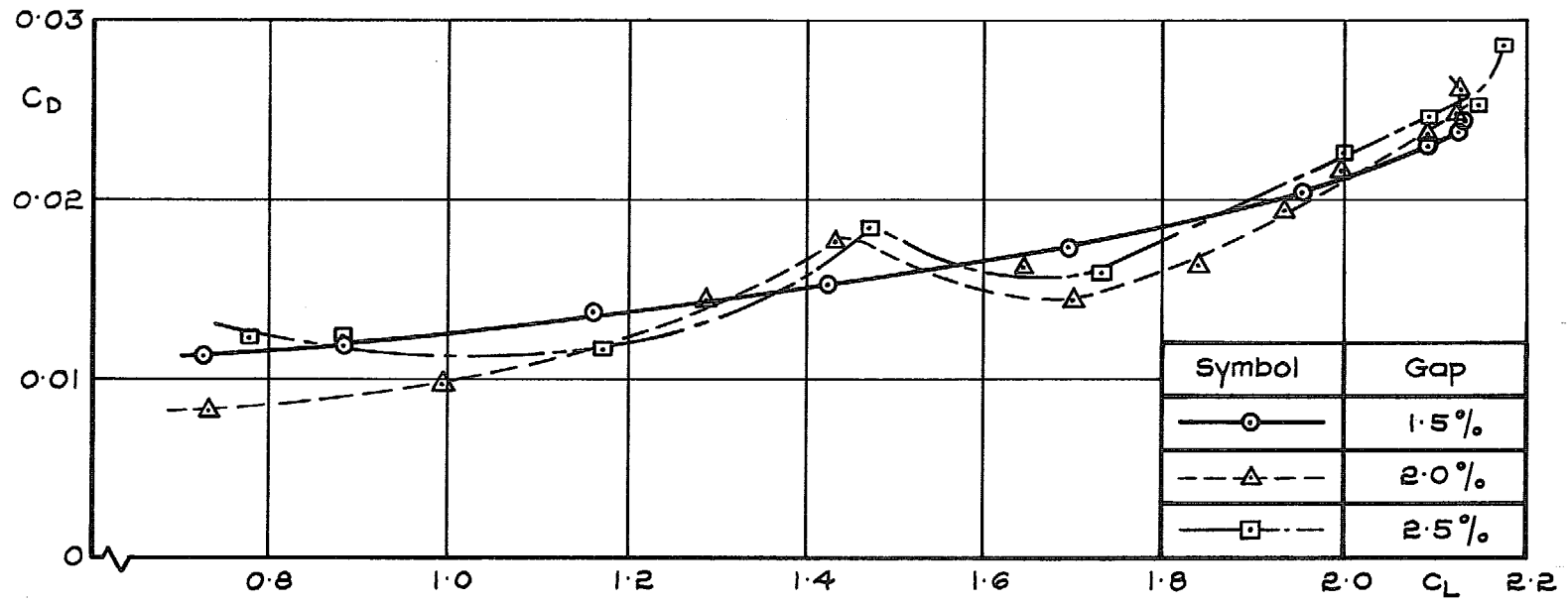
FIG. 13. Variation of sectional drag with lift and gap. Flap deflection 10°, plain leading edge.

Symbol	Gap
— –△– —	1·5%
—○—	2·0%
— –□– —	2·5%
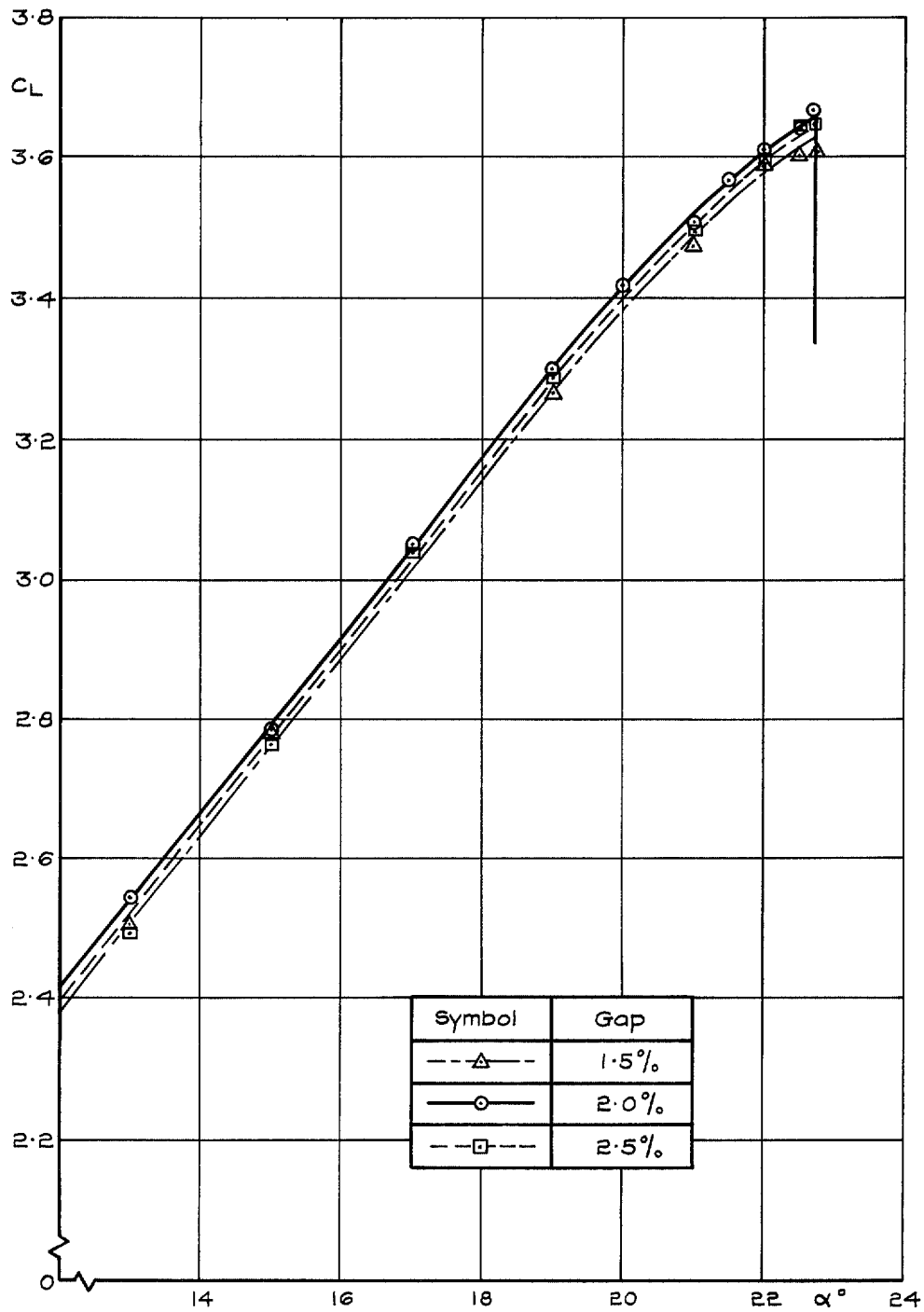
FIG. 14.   Effect of gap on lift. Flap deflection 10°, slatted leading edge.
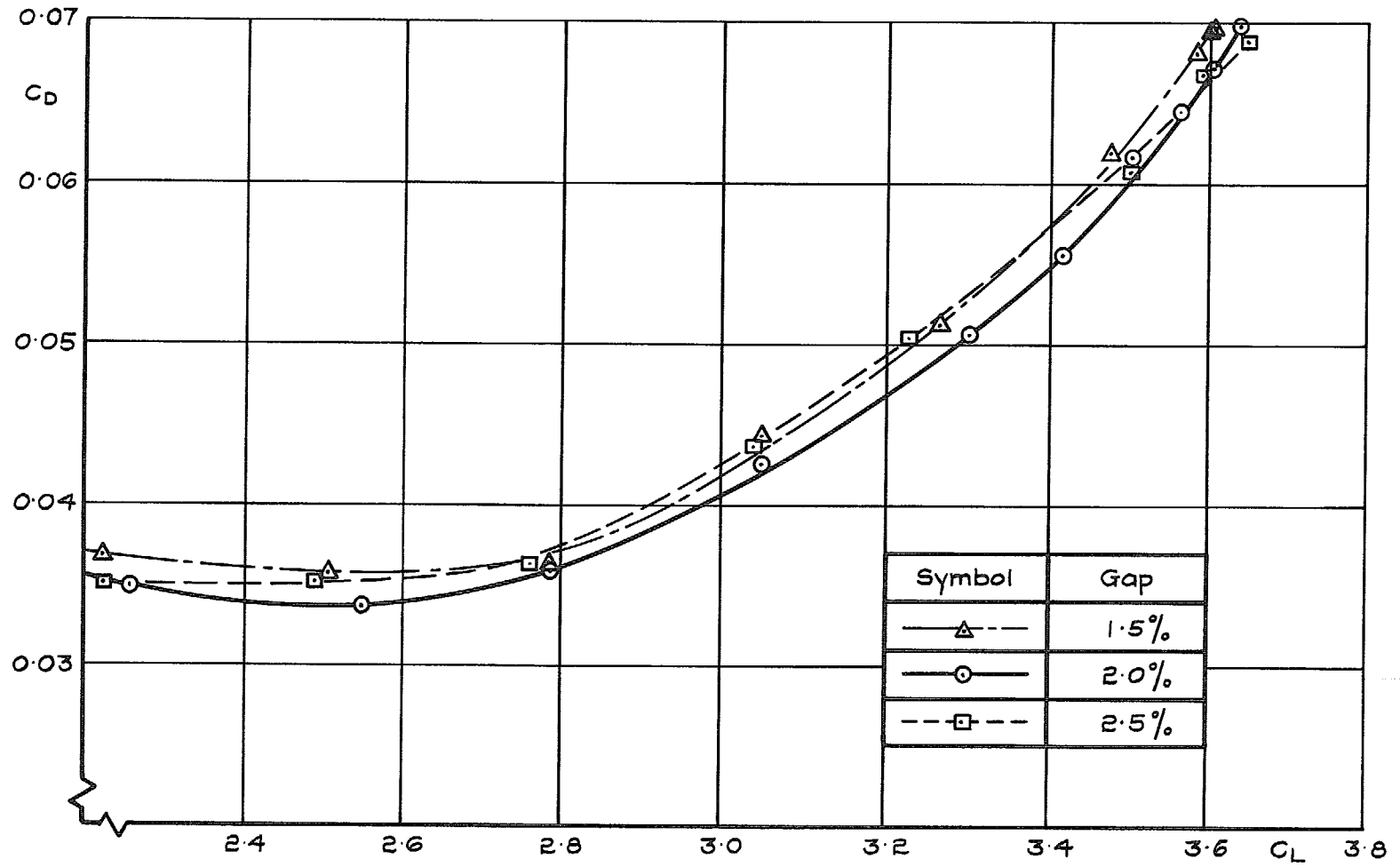
FIG. 15.   Variation of sectional drag with lift and gap. Flap deflection 10°, slatted leading edge.
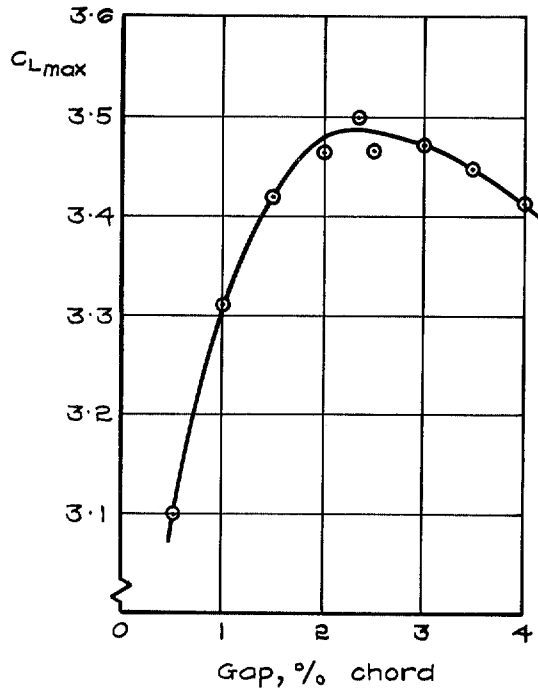
a   Drooped   leading   edge ,   flap   deflection   30°
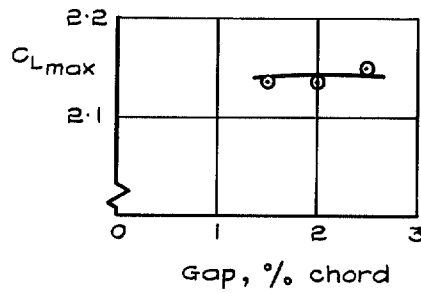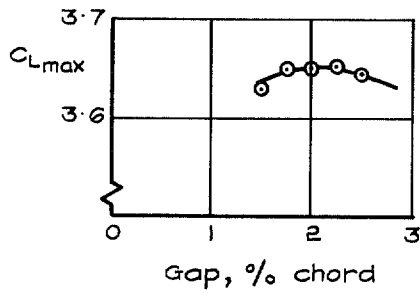
i   Slatted   leading   edge   ii   Plain   leading   edge

b   Flap   deflection   10°

FIG. 16 a. & b.   Effect of flap gap on maximum lift.
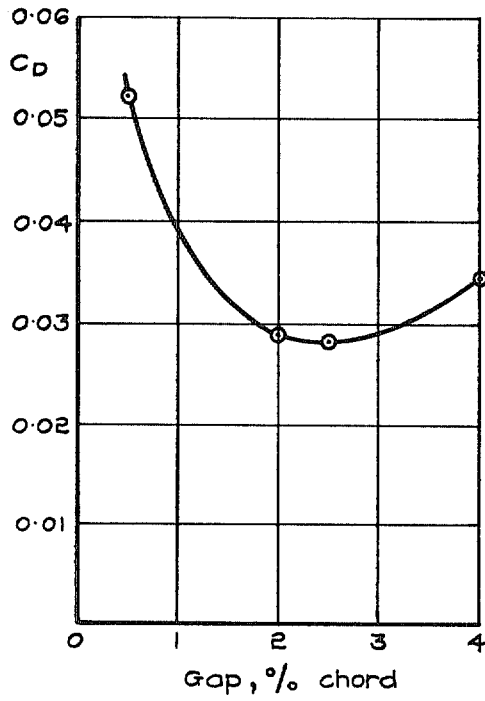
41

a   Drooped   leading   edge ,   flap   deflection   30°
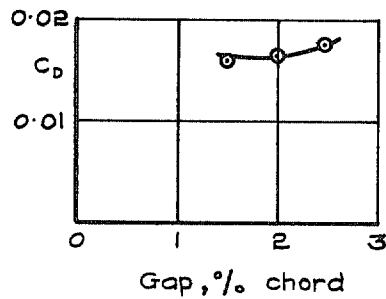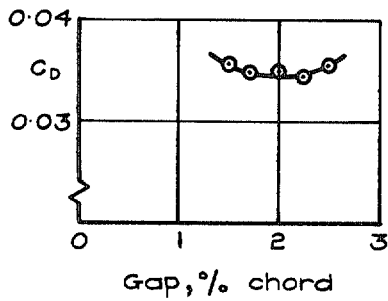
i   Slatted   leading   edge   ii   Plain   leading   edge

b   Flap   deflection   10°

FIG. 17 a. & b.   Effect of flap gap on drag at 70 % maximum lift.

42
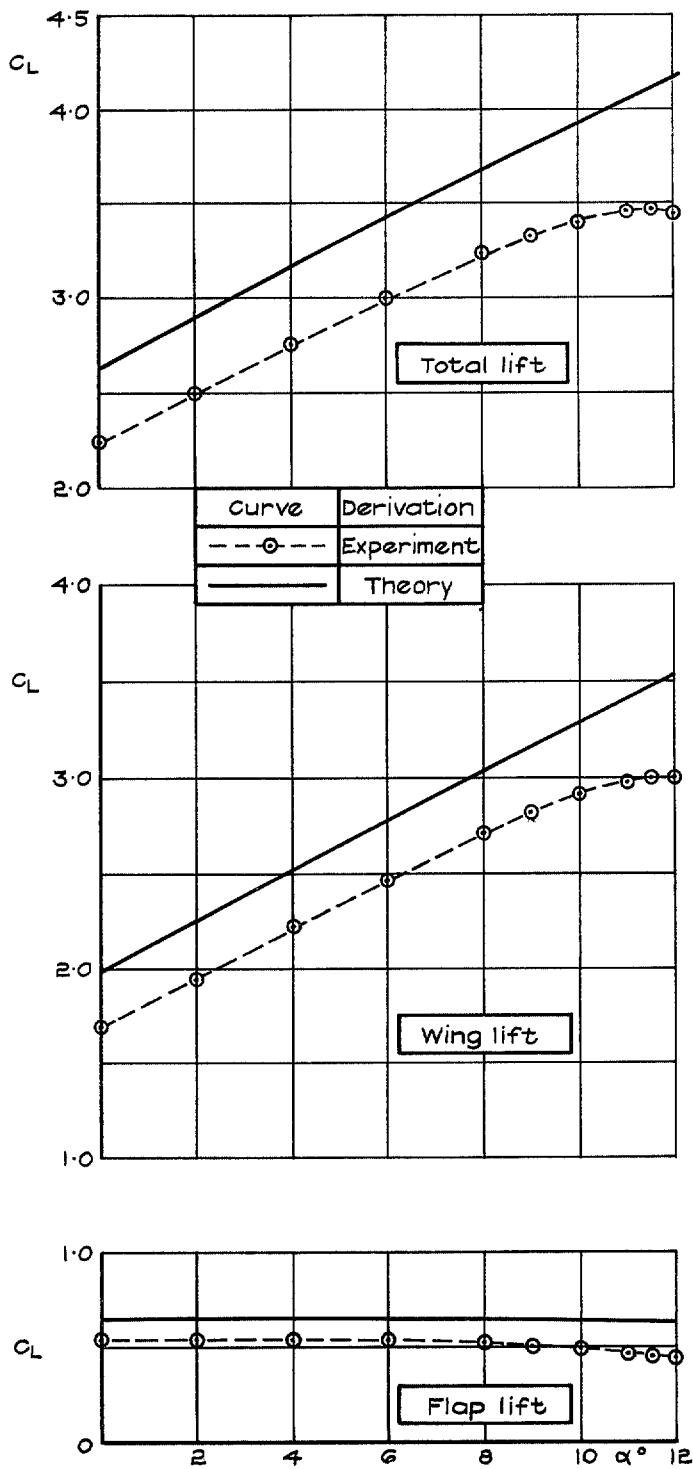
FIG. 18.   Variation of lift with incidence; fixed flap position. Flap deflection 30°.
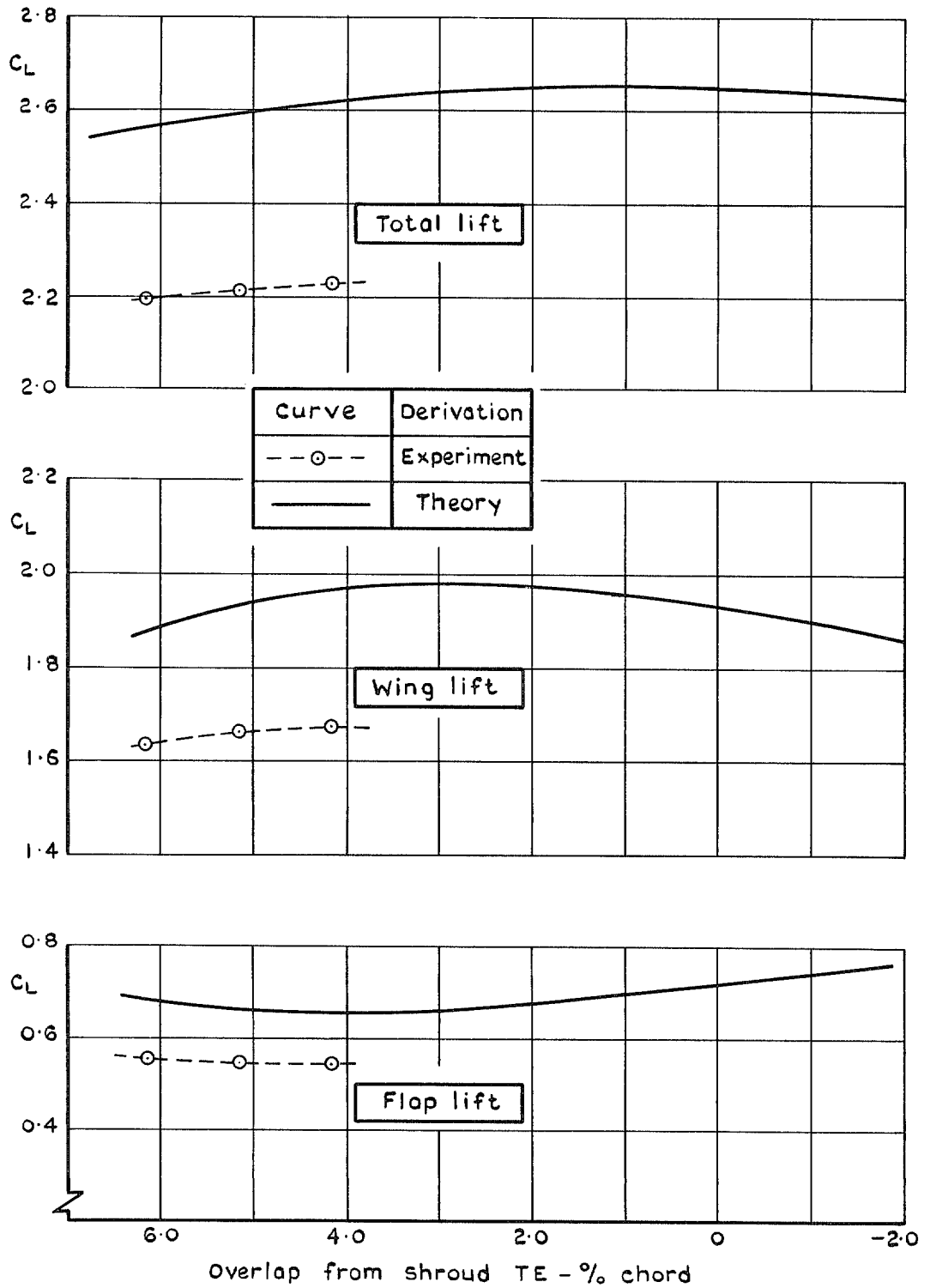
FIG. 19.   Variation of lift with overlap at zero incidence. Flap deflection 30°.
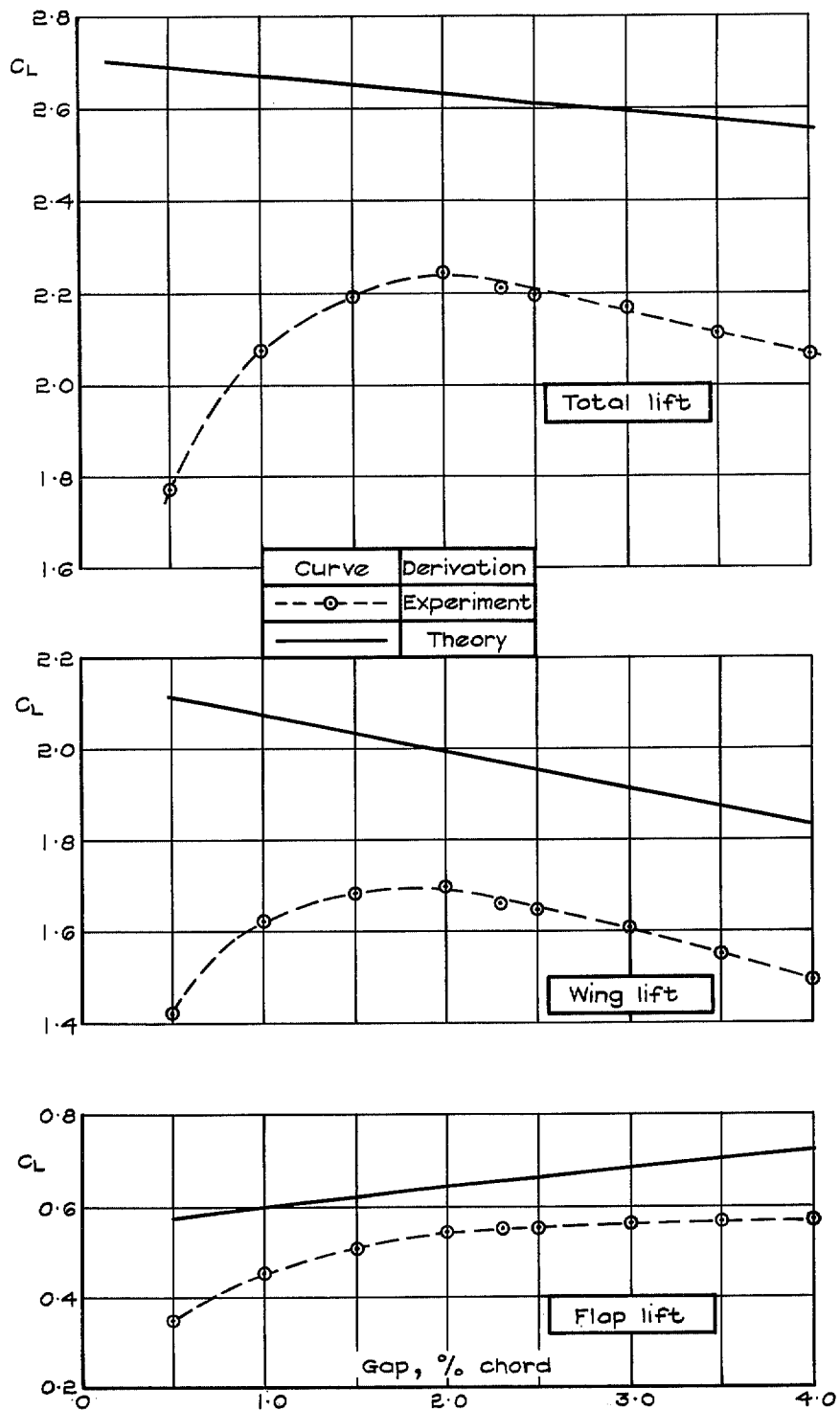
Fig. 20.   Variation of lift with gap, at zero incidence. Flap deflection 30°.
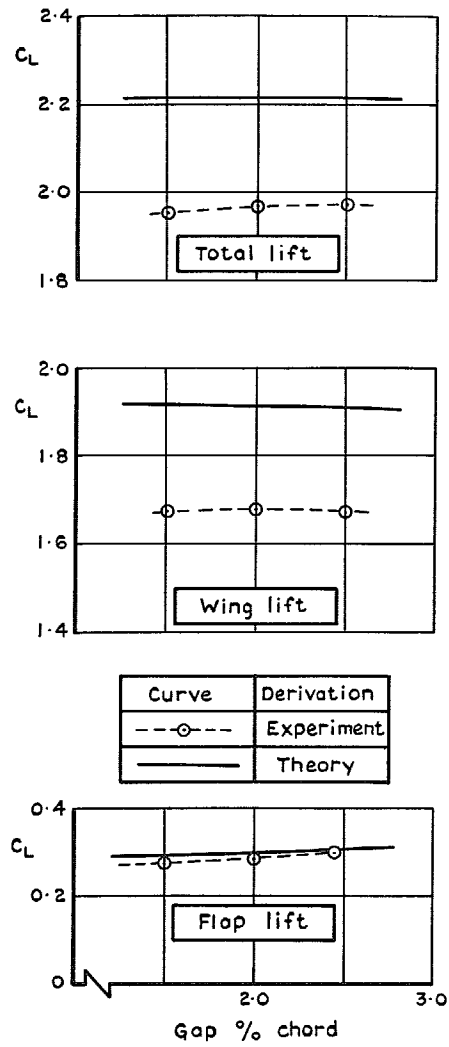
FIG. 21. Variation of lift with gap, angle of incidence 9°, flap deflection 10°, plain leading edge.
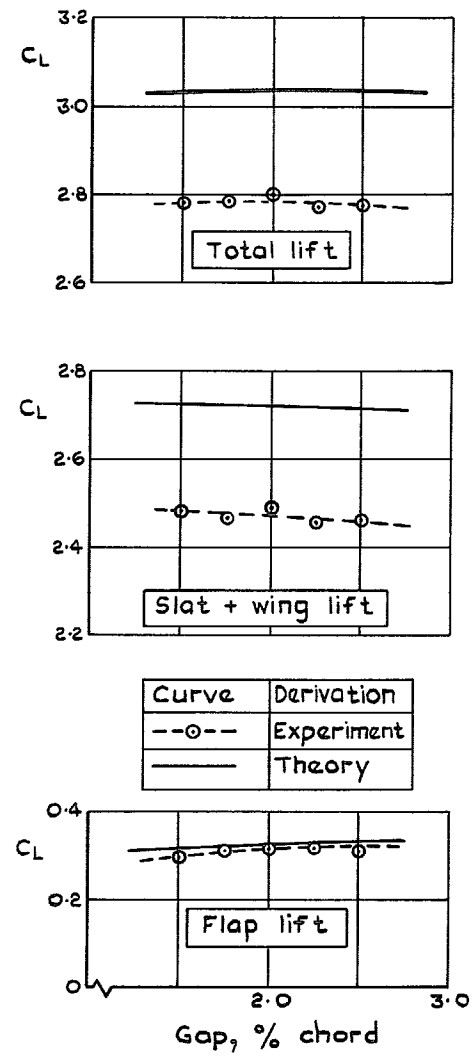
FIG. 22. Variation of lift with gap, angle of incidence 15°, flap deflection 10°, slatted leading edge.
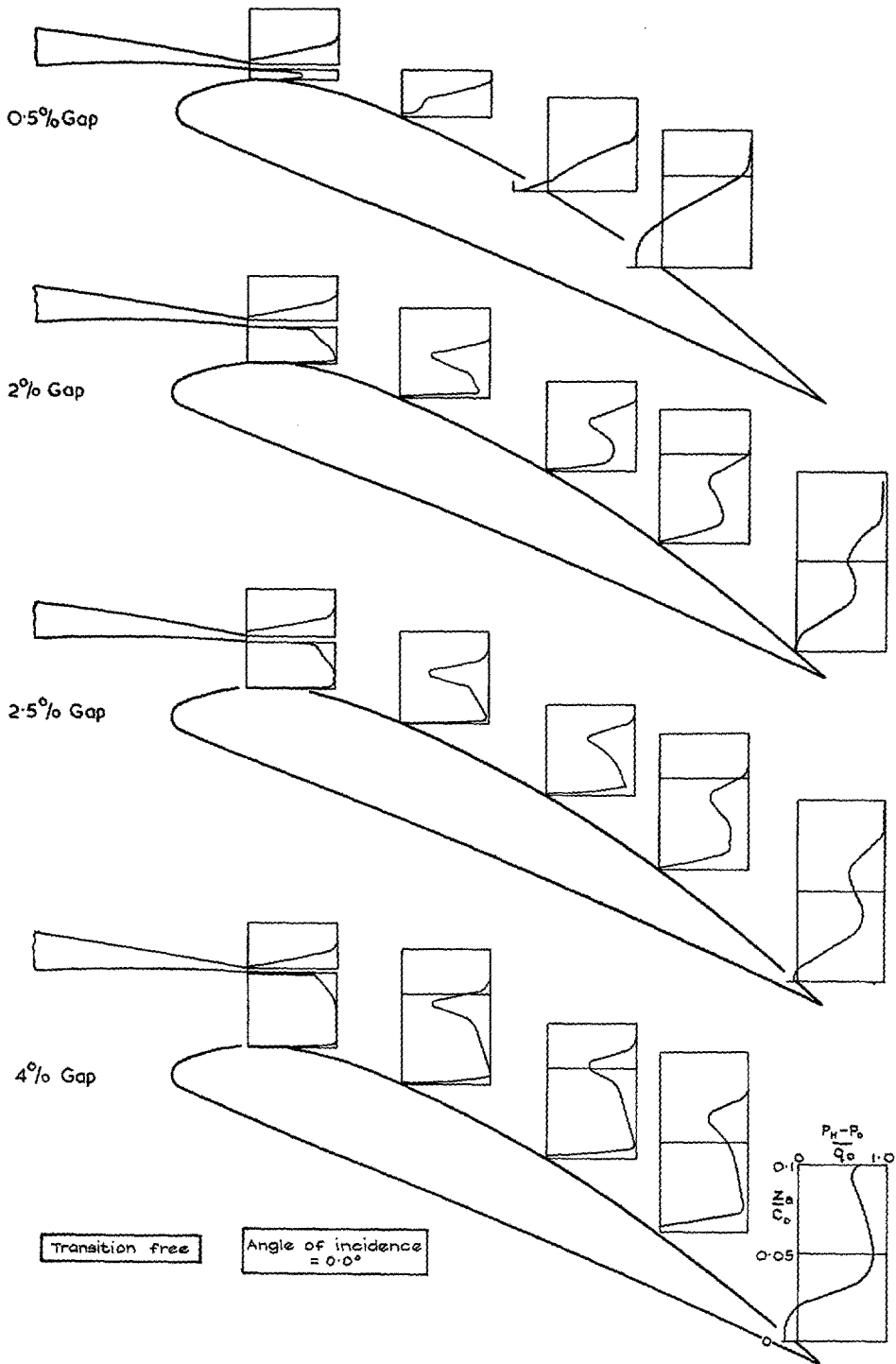
FIG. 23. Total head distribution in flow over flap, at 30° deflection.

1·5 %o Gap

2·0 %o Gap

2·5 %o Gap

Curve	Transition
———	Free
- - - -	Fixed

Angle of incidence
= 9·0°

$\dfrac{P_H - P_o}{q_o}$

$\dfrac{z_B}{c_o}$
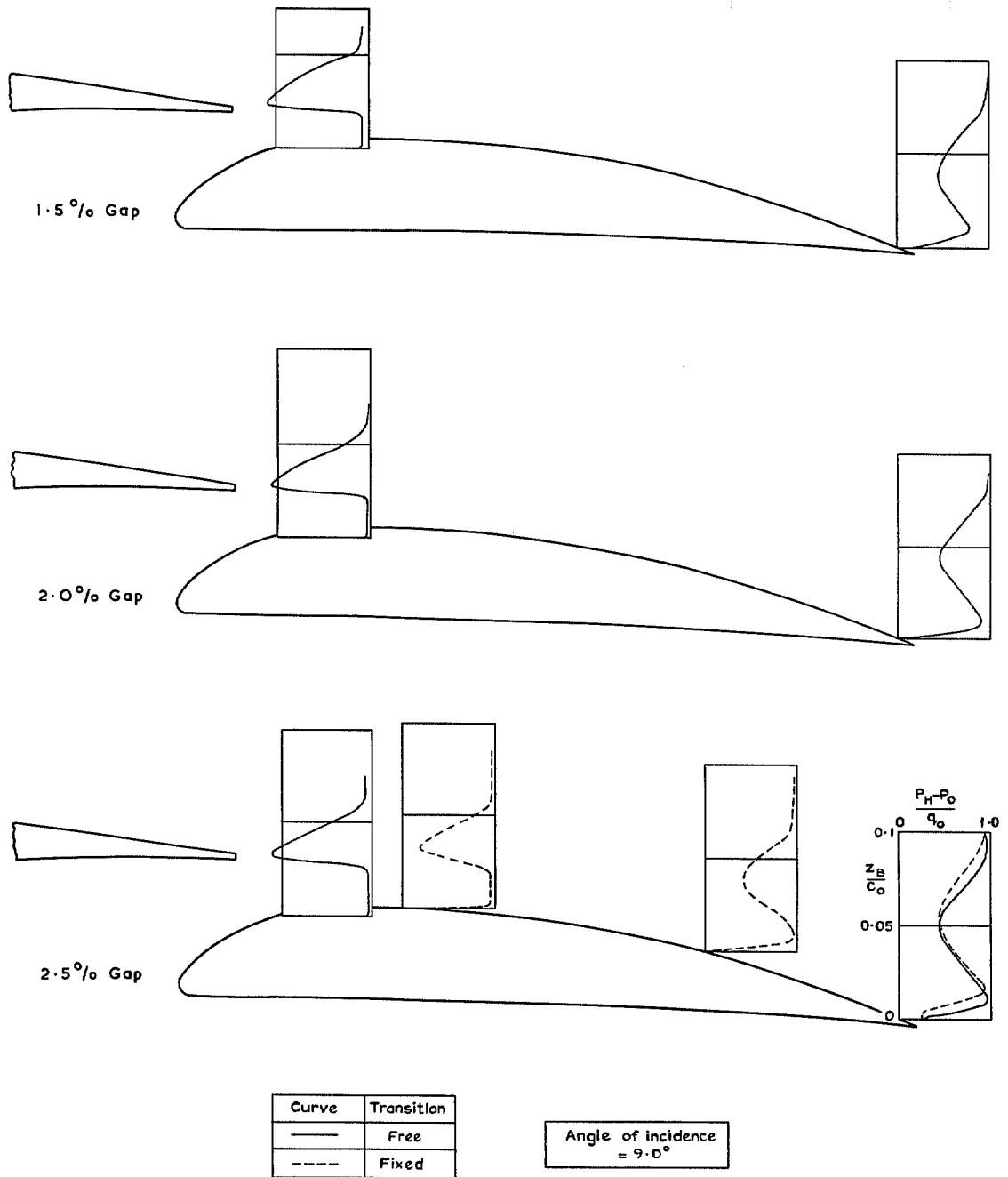
Fig. 24. Total head distribution in flow over flap at 10° deflection, plain leading edge.

Fig. 25

$$\frac{P_H - P_0}{q_0}$$

$$\frac{Z_B}{C_0}$$

Angle of incidence = 15°
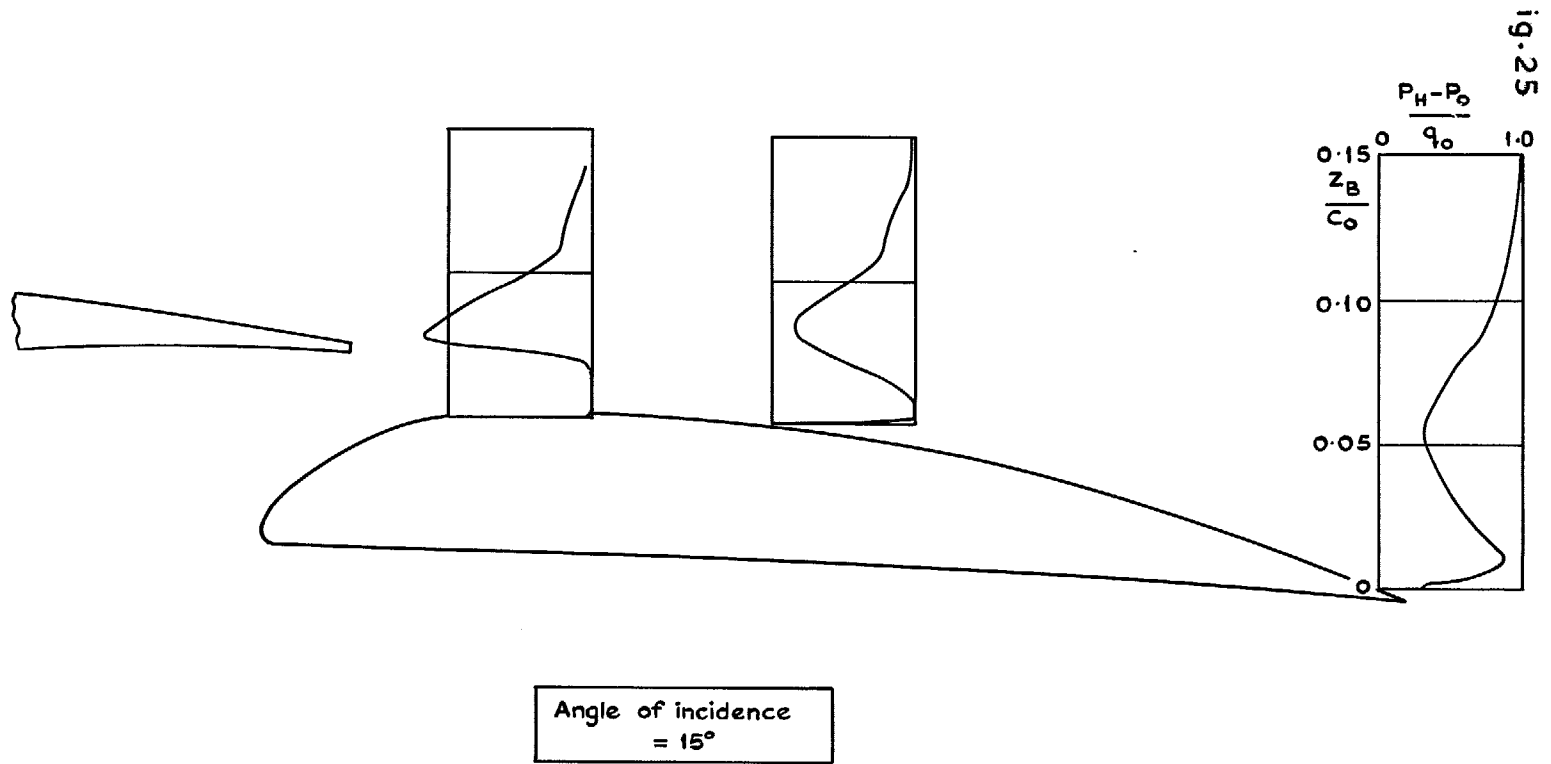
FIG. 25.   Total head distribution in flow over flap behind slatted leading edge.
Flap deflection 10°, flap gap 2%.

Curve	Angle of incidence
———	0°
– – –	8°

$$\frac{P_H - P_O}{q_0}$$

$\frac{Z_B}{C_0}$

Transition free
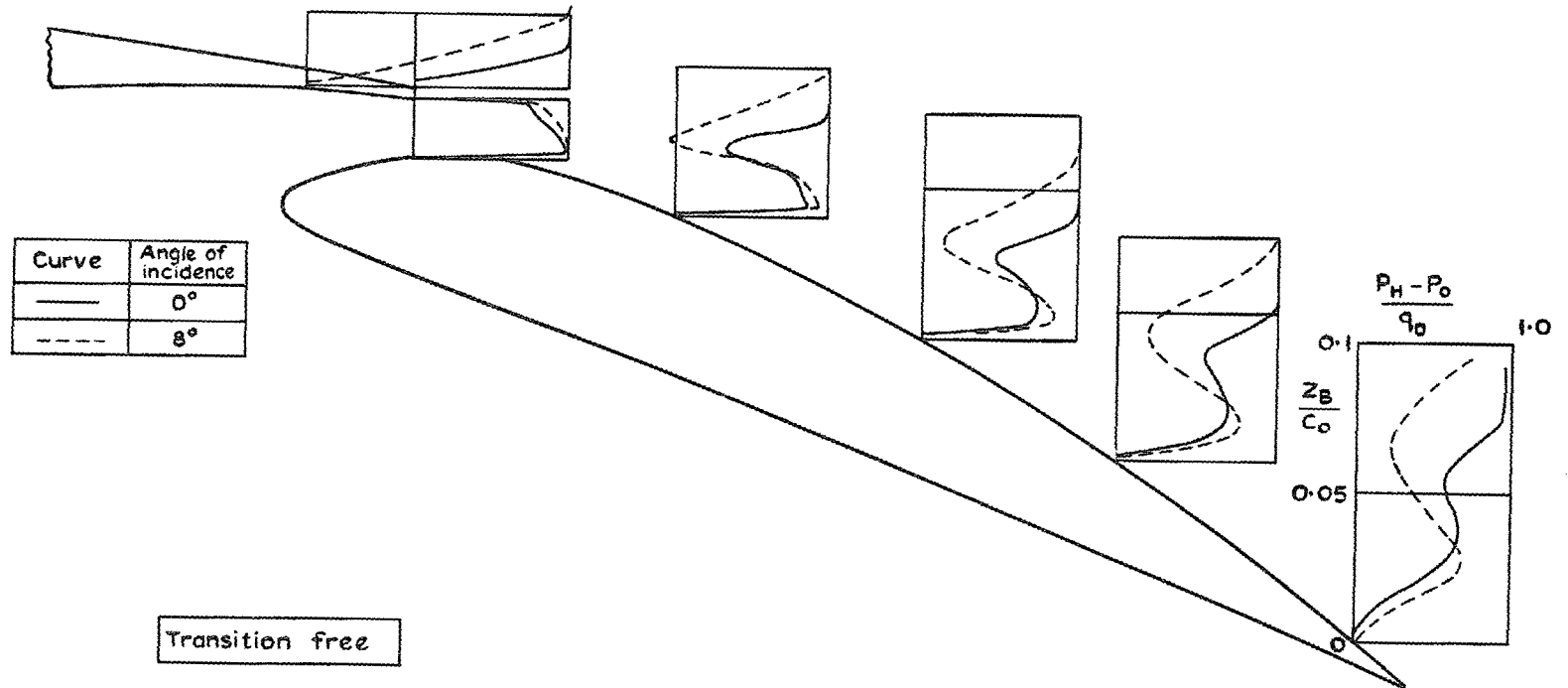
FIG. 26. Effect of angle of incidence on total head distribution in flow above flap.
Flap deflection 30°. Flap gap 2%.

Curve	Angle of incidence
——————	$0°$
-----	$9°$

Transition free
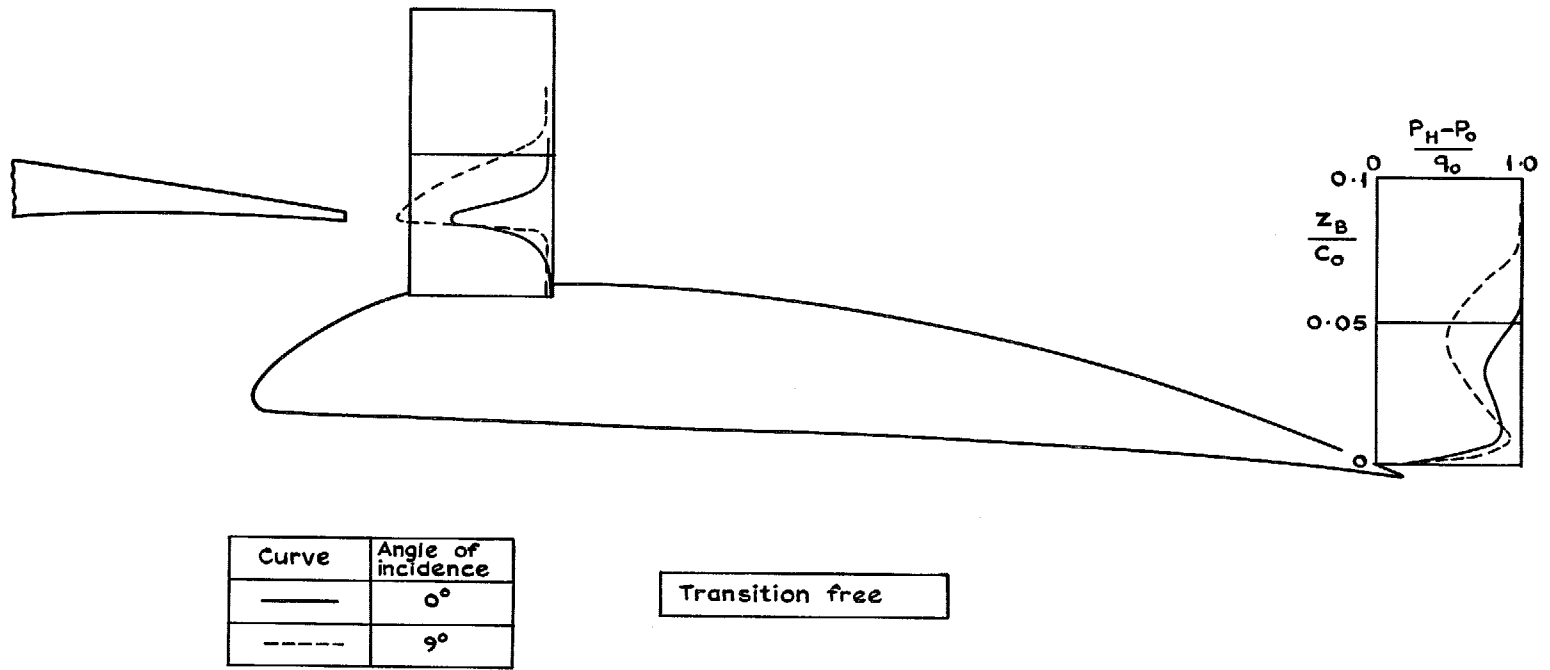
FIG. 27. Effect of angle of incidence on total head distribution in flow over flap.
Flap deflection 10°, Flap gap 2%, plain leading edge.
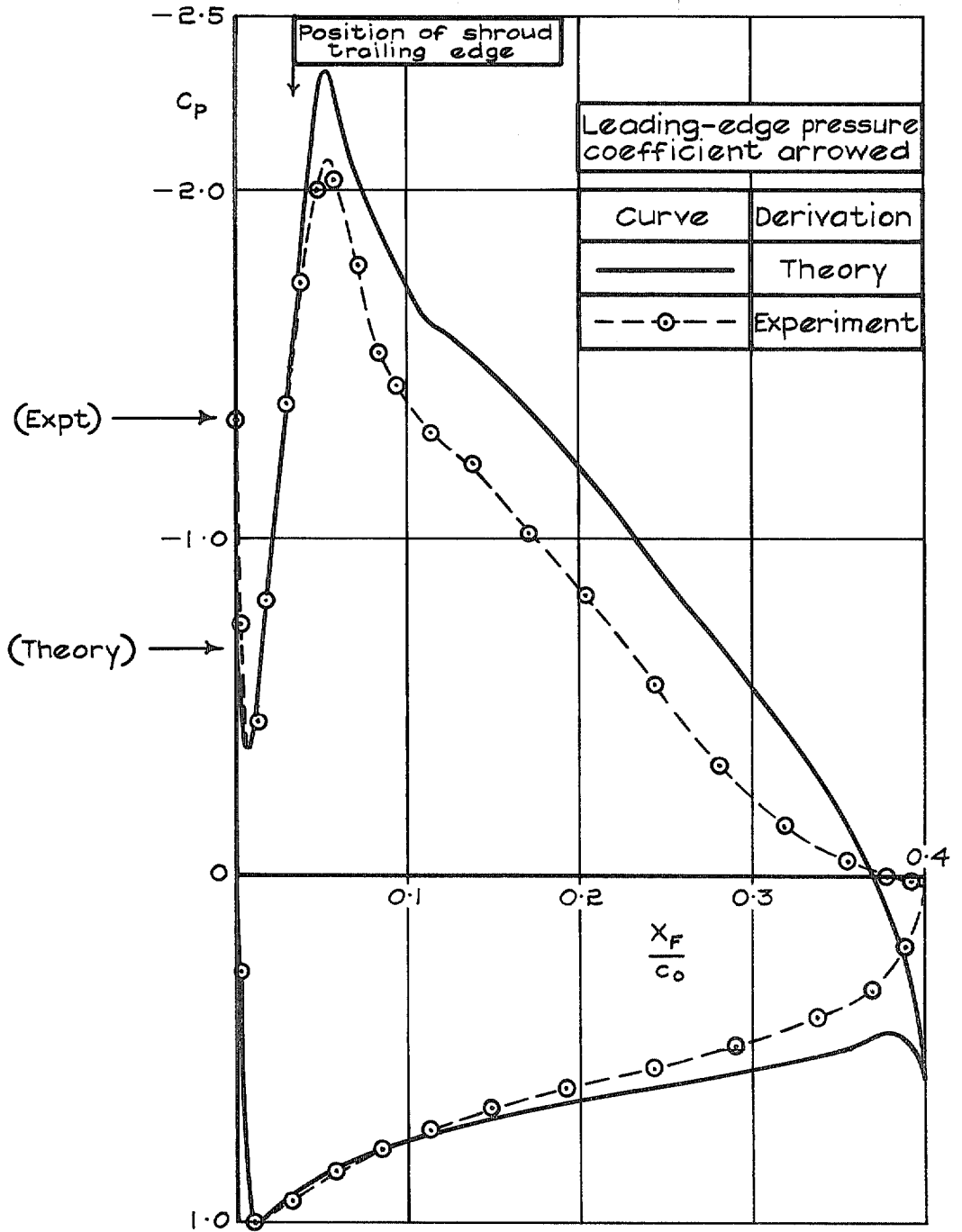
FIG. 28. Comparison of experimental and theoretical pressure distribution. Flap deflection 30°, flap gap 2%, angle of incidence 0°.
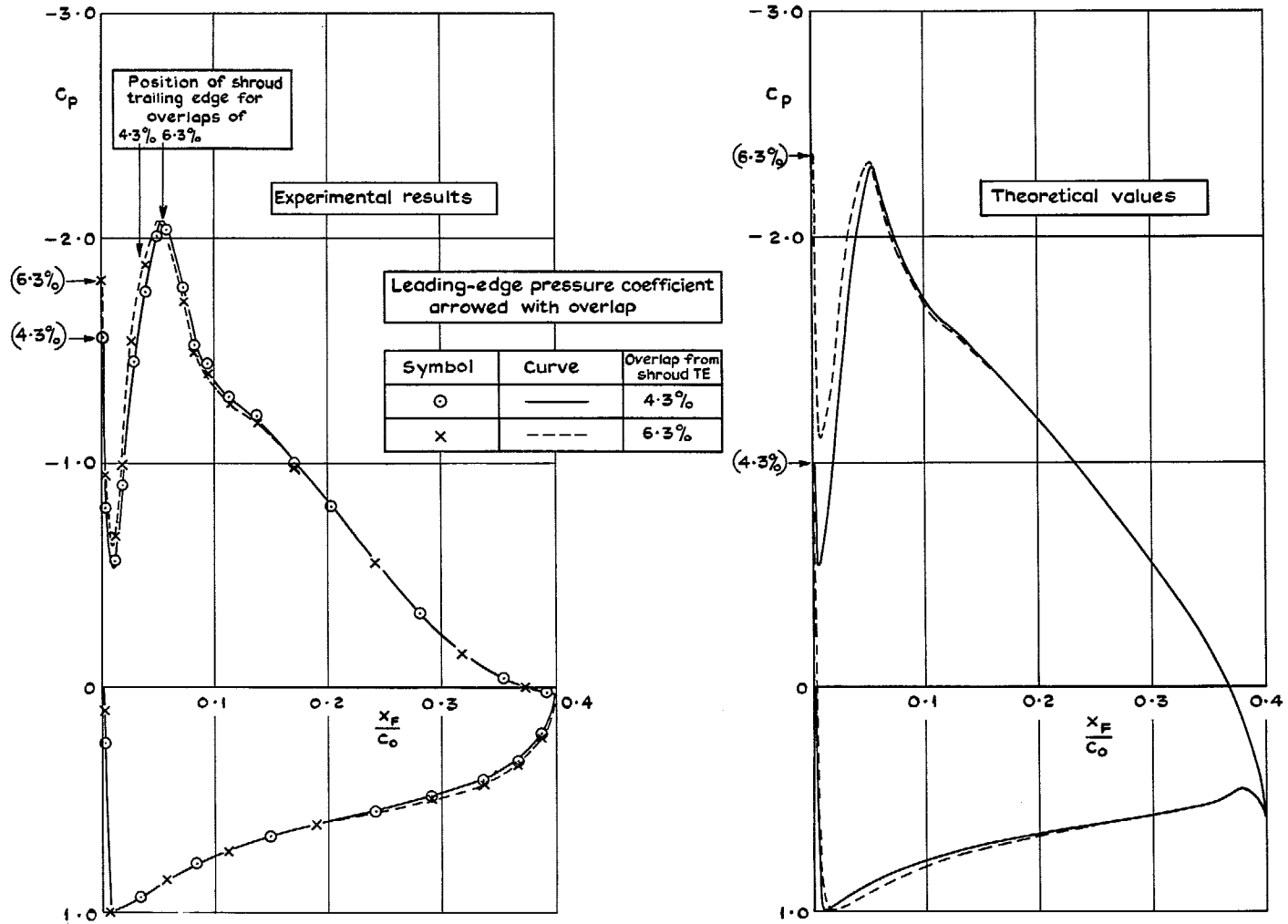
FIG. 29. Experimental and theoretical effect of overlap on flap pressure distribution.
Flap deflection 30°, angle of incidence 0°.
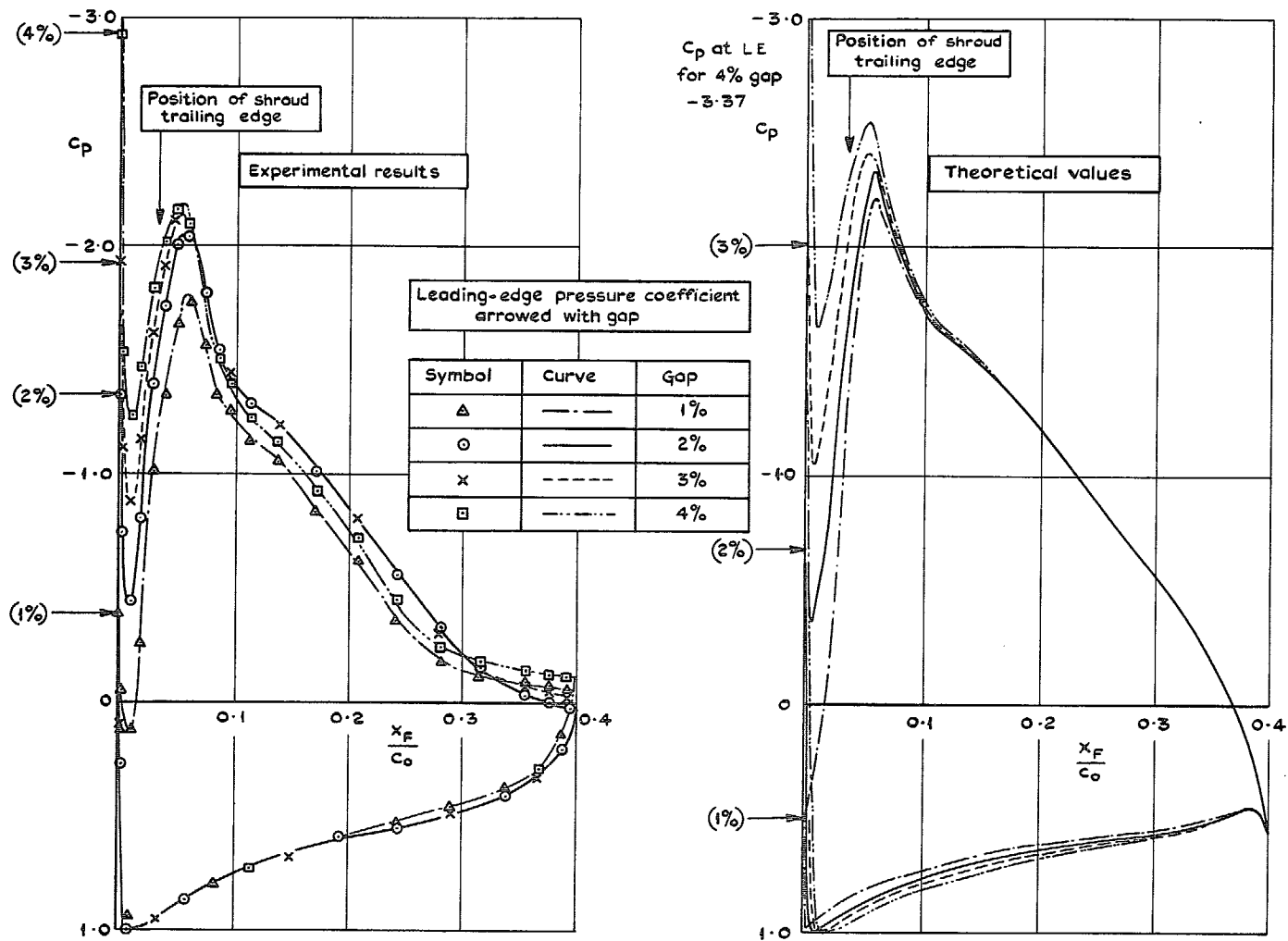
FIG. 30. Experimental and theoretical effect of gap on flap pressure distribution.
Flap deflection 30°, angle of incidence 0°.
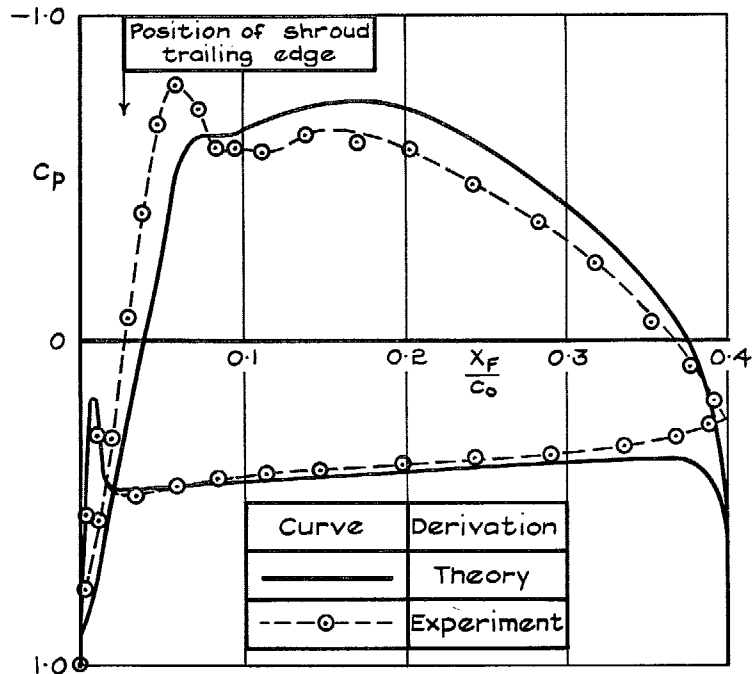
FIG. 31. Comparison of experimental and theoretical pressure distributions. Flap deflection 10°, flap gap 2%, angle of incidence 9°, plain leading edge.
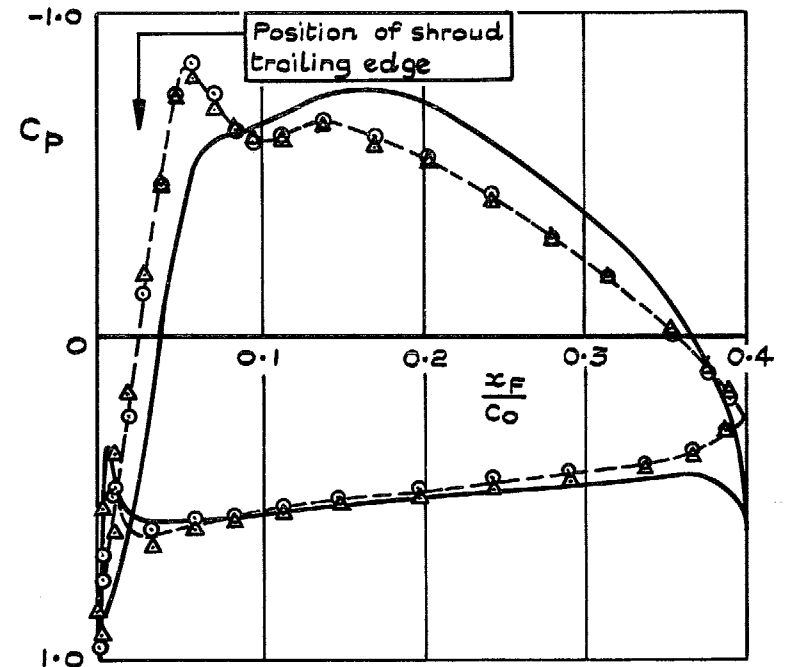
FIG. 32. Comparison of experimental and theoretical pressure distributions. Flap deflection 10°. flap gap 2%, angle of incidence 15°, slatted leading edge.
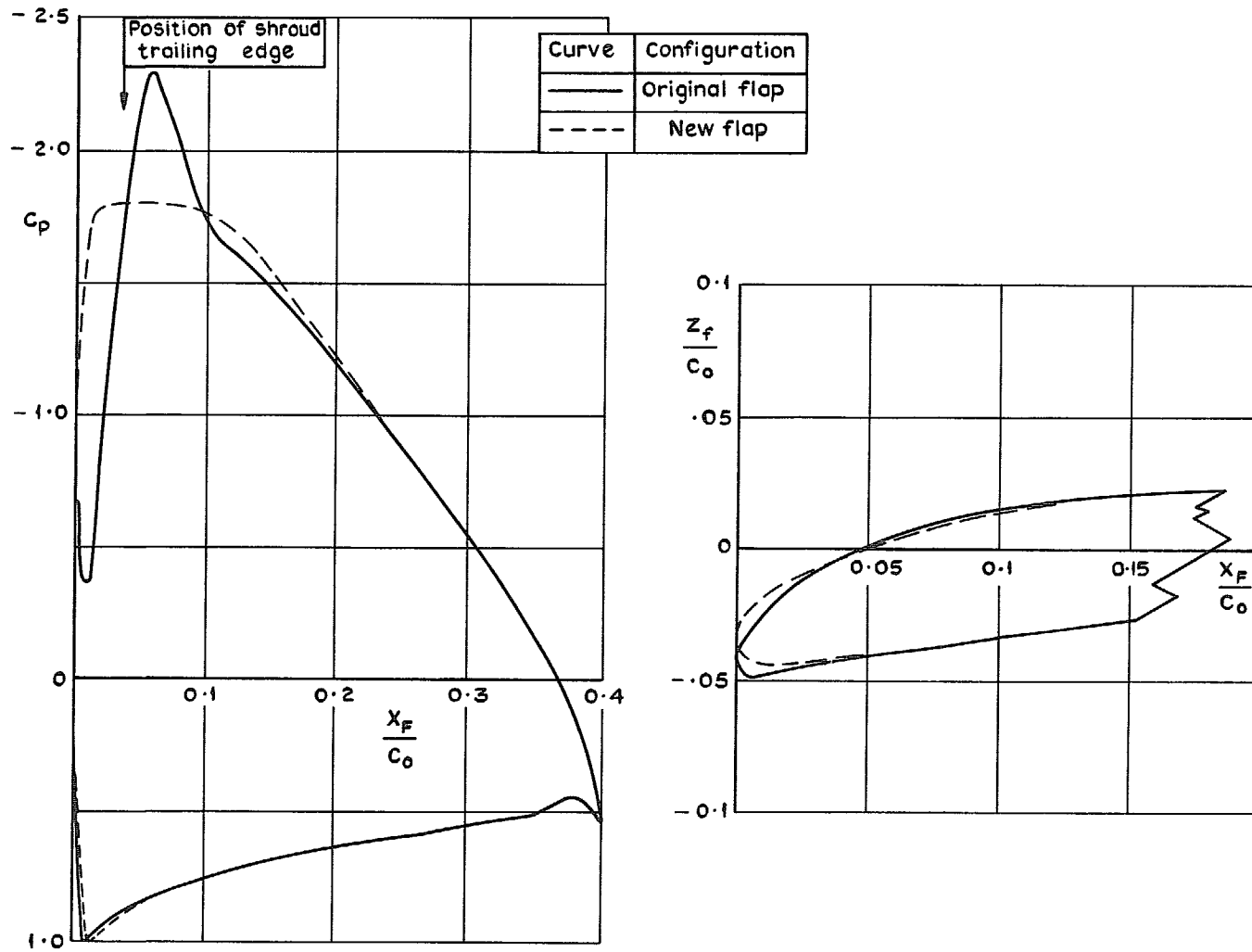
FIG. 33. Comparison of pressure distribution and shape for original and new flap.
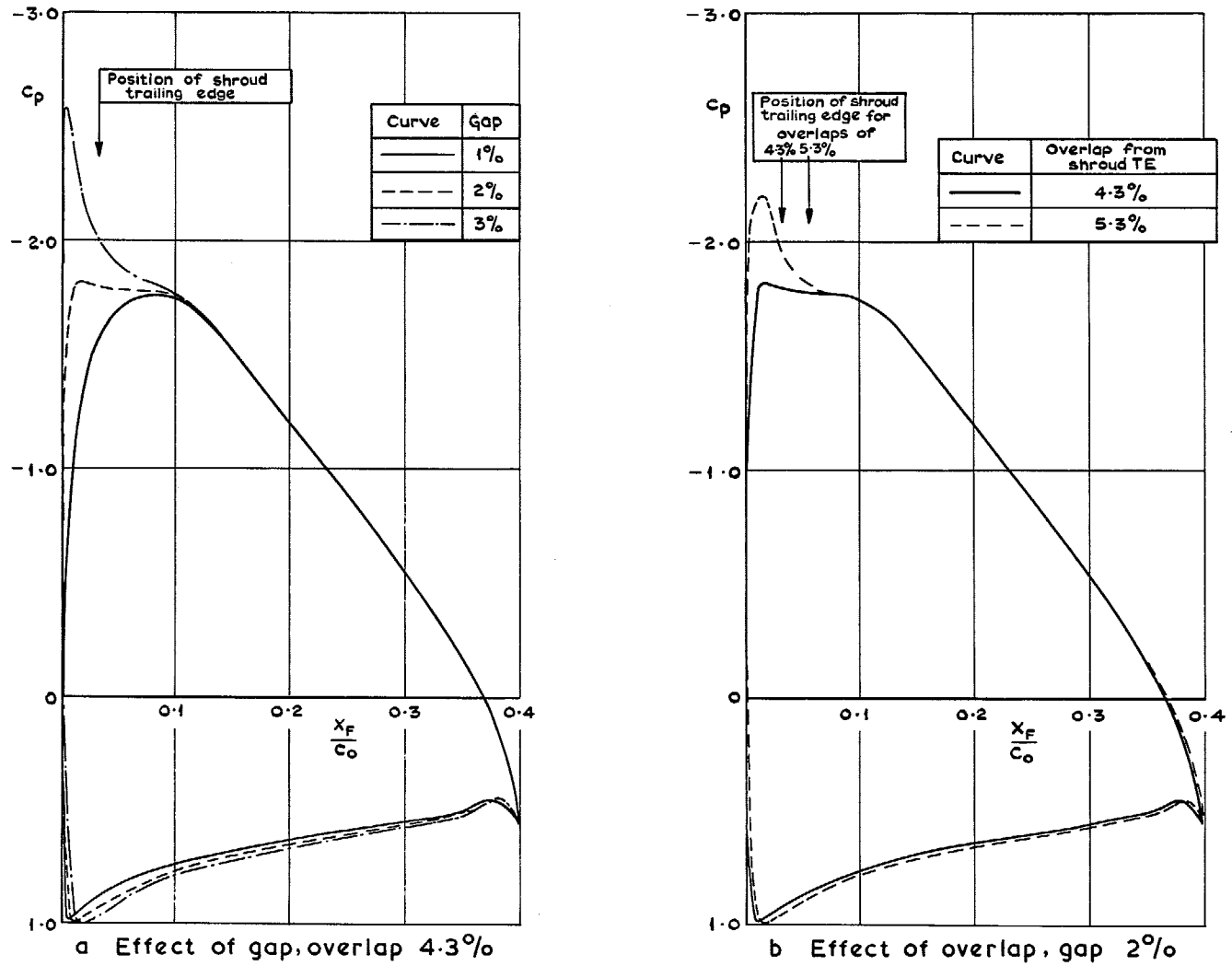
FIG. 34 a. & b.   Effect of gap and overlap on theoretical pressure distributions for new flap.
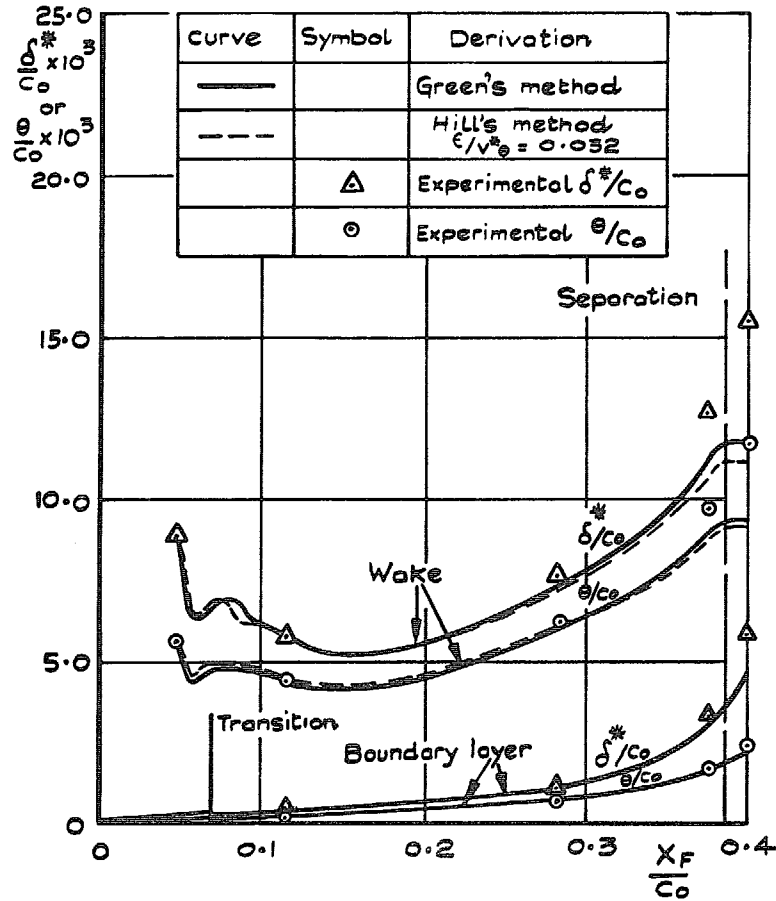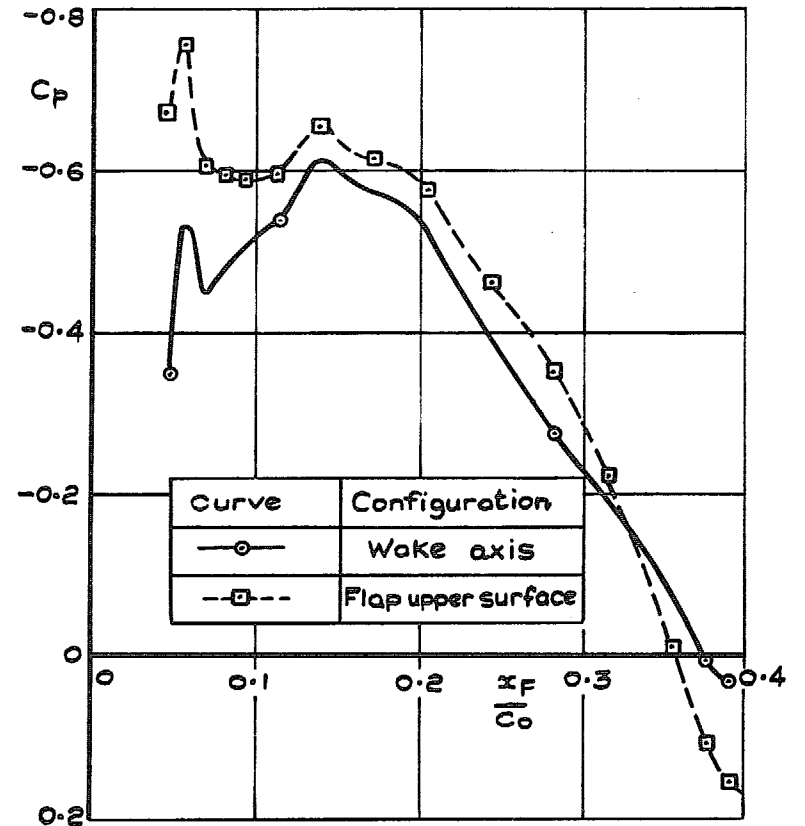
Fig. 35 a. & b. Wake and boundary layer developments, and corresponding pressure distributions.

Curve	Symbol	Derivation
– – – –		δ^*/c_o Calculated by Green's method
——		θ/c_o Calculated by Green's method
	$\triangle$	Experimental value of δ^*/c_o
	$\odot$	Experimental value of θ/c_o
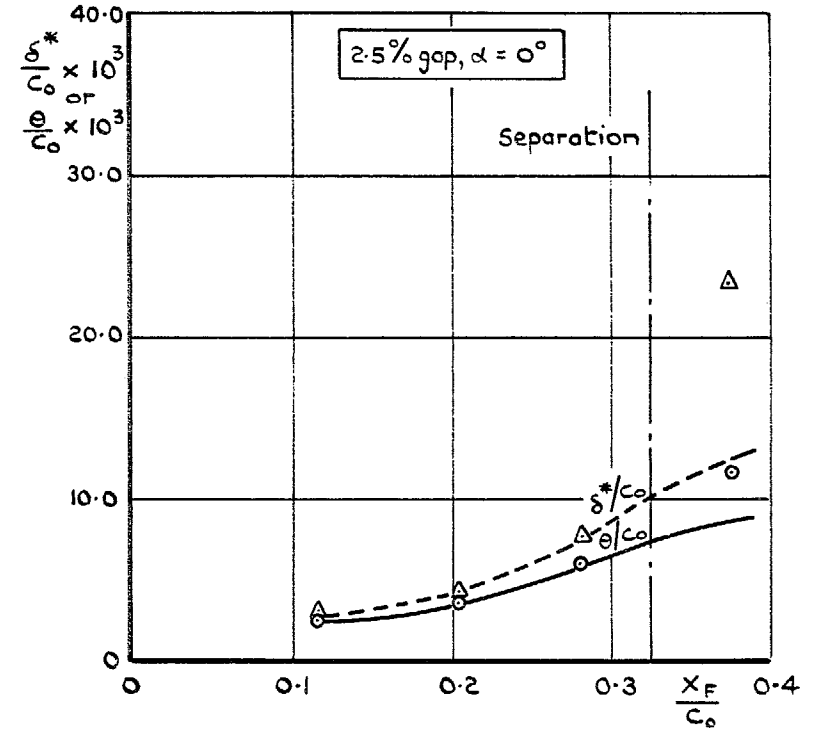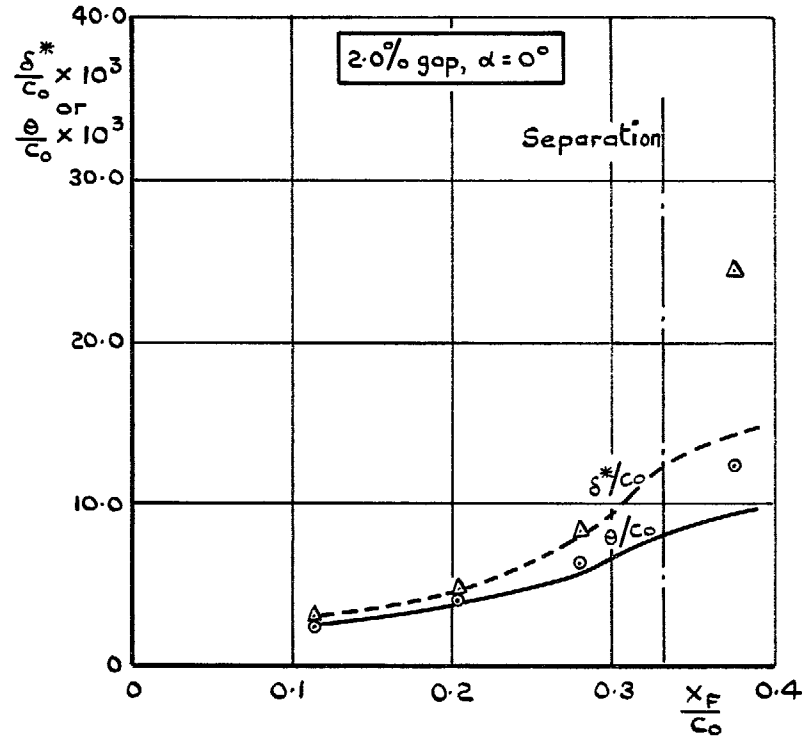
FIG. 36. Development of viscous layers over flap. Flap deflection 30°.

Curve	Symbol	Derivation
– – – – –		δ^*/c_0 Calculated by Green's method
————		θ/c_0 Calculated by Green's method
	△	Experimental value of δ^*/c_0
	◉	Experimental value of θ/c_0
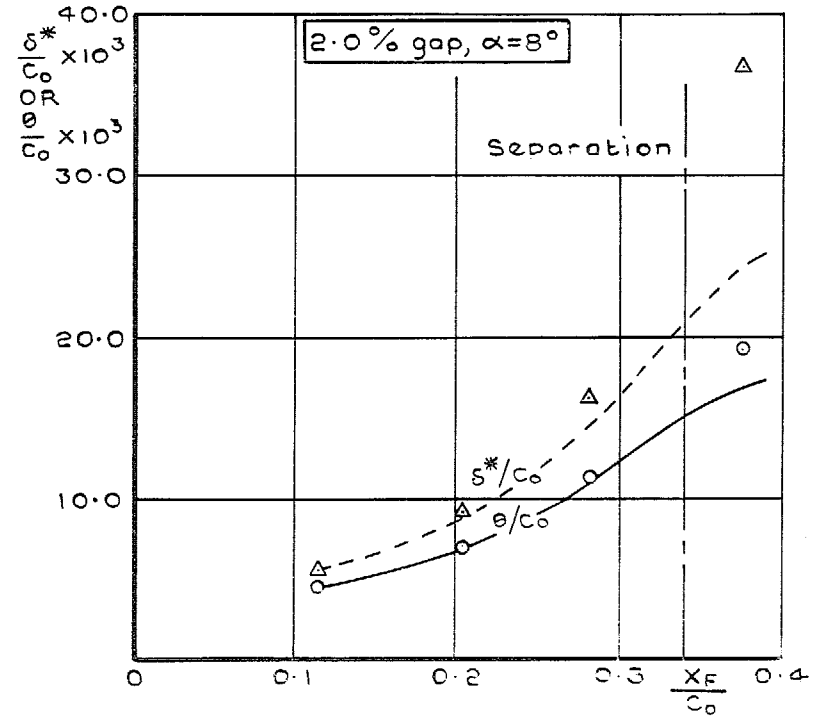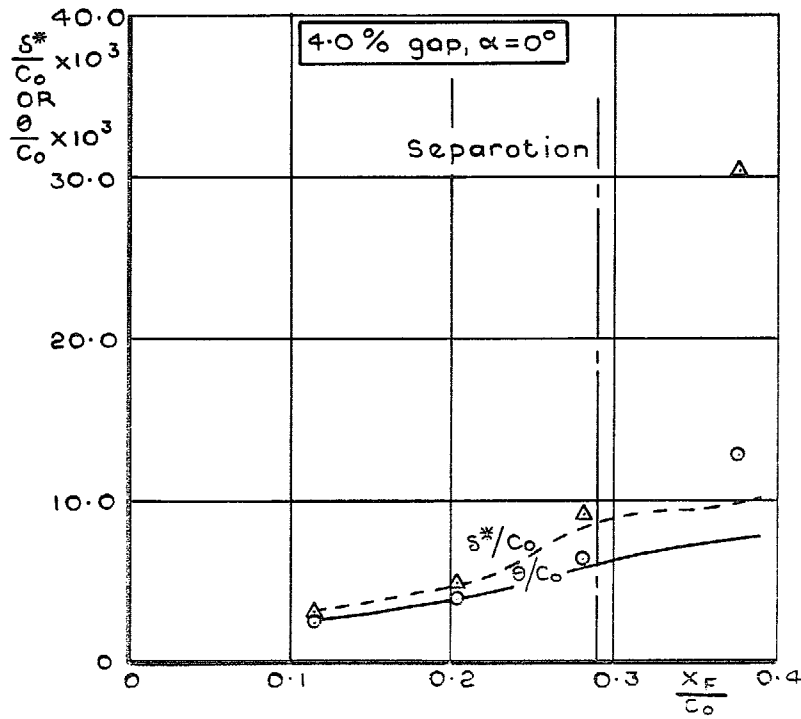
FIG. 37.   Development of viscous layers over flap. Flap deflection 30°.

Curve	Symbol	Derivation
― ― ― ―		δ^*/c_0 calculated by Green's method
————		θ/c_0 calculated by Green's method
	△	Experimental value of δ^*/c_0
	⊙	Experimental value of θ/c_0

FIG. 38.   Development of viscous layers over flap. Flap deflection 10°, plain leading edge.

Curve	Symbol	Derivation
— — — —		δ^*/c_0 calculated by Green's method
———————		θ/c_0 calculated by Green's method
	△	Experimental value of δ^*/c_0
	⊙	Experimental value of θ/c_0

FIG. 39.   Development of viscous layers over flap. Flap deflection 10°, plain leading edge.

Curve	Symbol	Derivation
– – – –		δ^*/c_0 calculated by Green's method
————		θ/c_0 calculated by Green's method
	△	Experimental value of δ^*/c_0
	⊙	Experimental value of θ/c_0

$$\frac{\delta^*}{c_0} \times 10^3 \text{ or } \frac{\theta}{c_0} \times 10^3$$

Gap = 2·0%, α = 0°

Transition

δ^*/c_0

θ/c_0

a Plain leading edge $\dfrac{x_F}{c_0}$

Gap = 2·0%, α = 15°

Transition

δ^*/c_0

θ/c_0
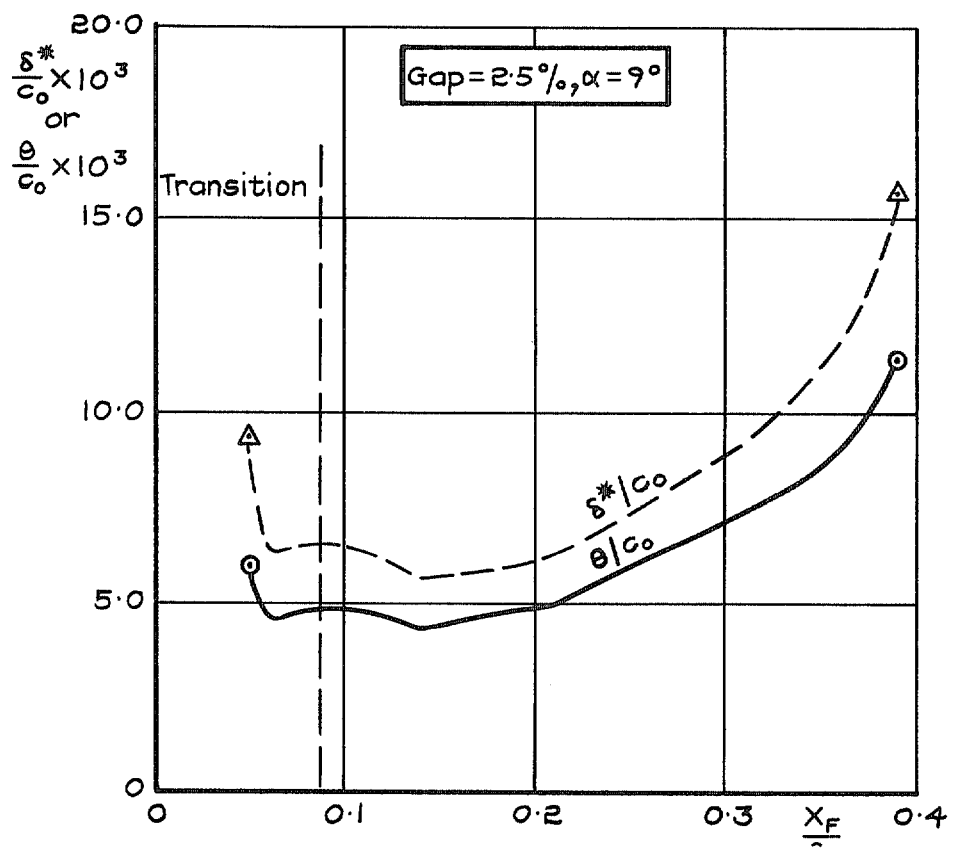
b Slatted leading edge $\dfrac{x_F}{c_0}$

FIG. 40 a. & b. Effect of leading-edge configuration on development of viscous layers over flap. Flap deflection 10°.

Curve	Symbol	Derivation
———————		Green's method from traverse at $X_F/c_o = 0.030$
– – – – –		Green's method from traverse at $X_F/c_o = 0.114$
	⊙	Measured by rectangular pitot tube
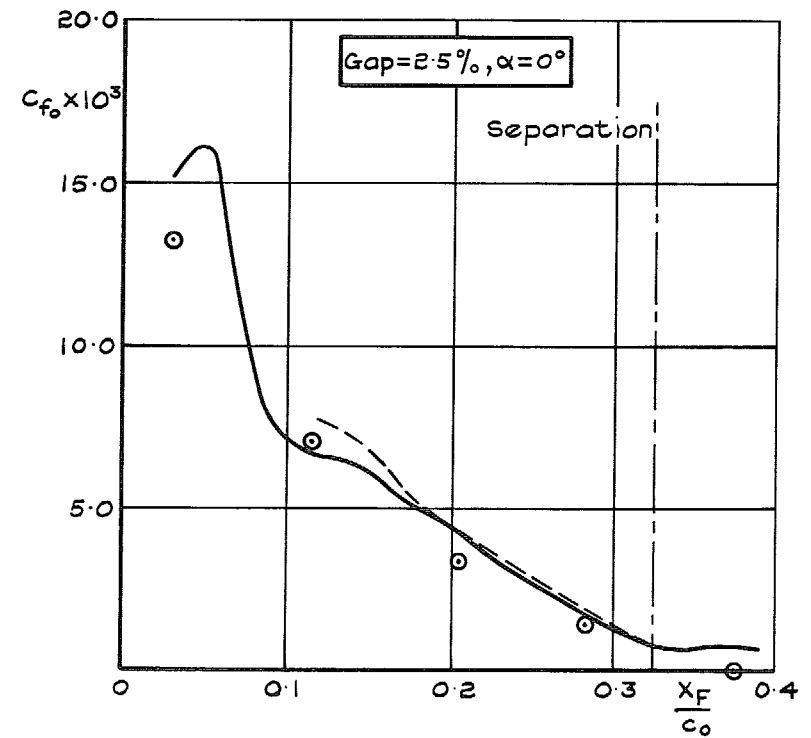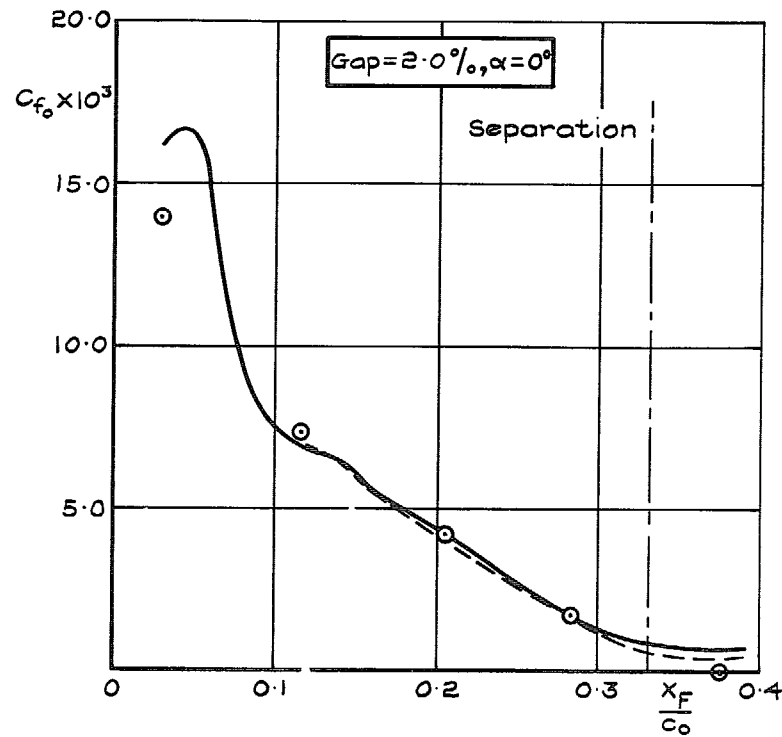
FIG. 41.   Skin-friction coefficient on flap upper surface. Flap deflection 30°.

Curve	Symbol	Derivation
————		Green's method from traverse at $X_F/c_o = 0.030$
– – – –		Green's method from traverse at $X_F/c_o = 0.114$
	⊙	Measured by rectangular pitot tube
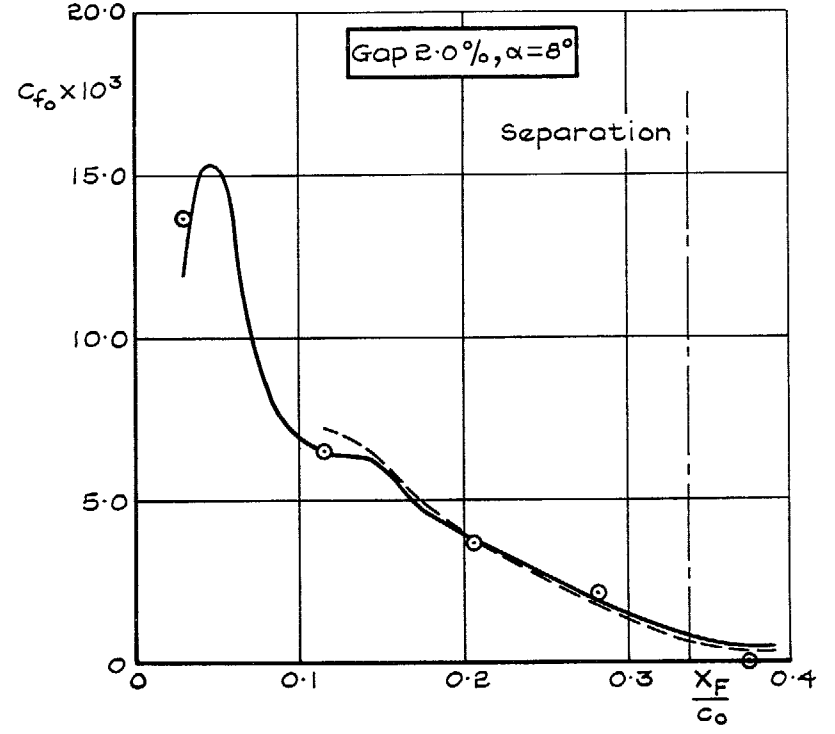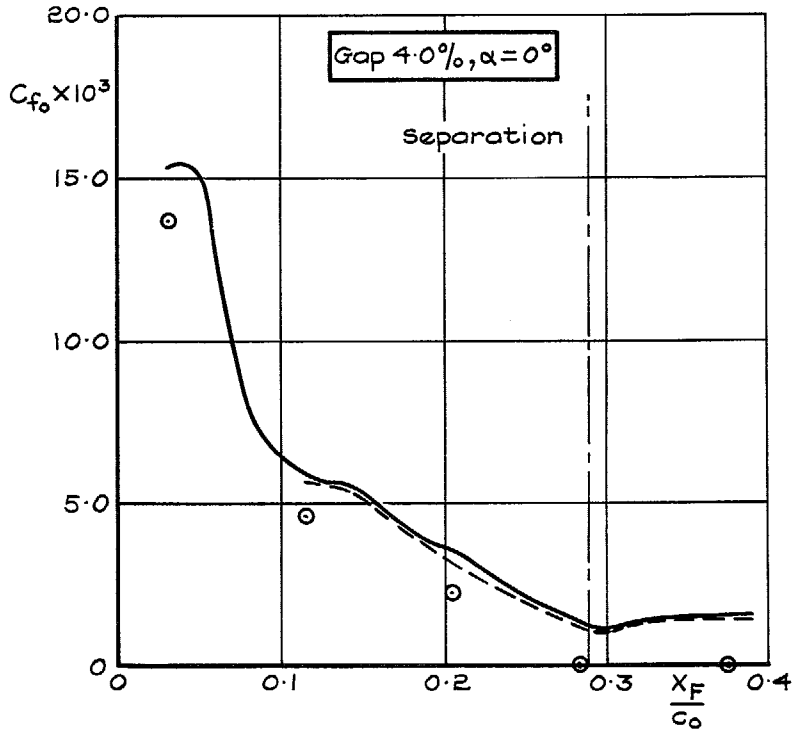
FIG. 42.   Skin-friction coefficient on flap upper surface. Flap deflection 30°.

Curve	Symbol	Derivation
	⊙	Measured by razor blade technique
——————		Thwaites' method for laminar flow, Green's method for turbulent flow
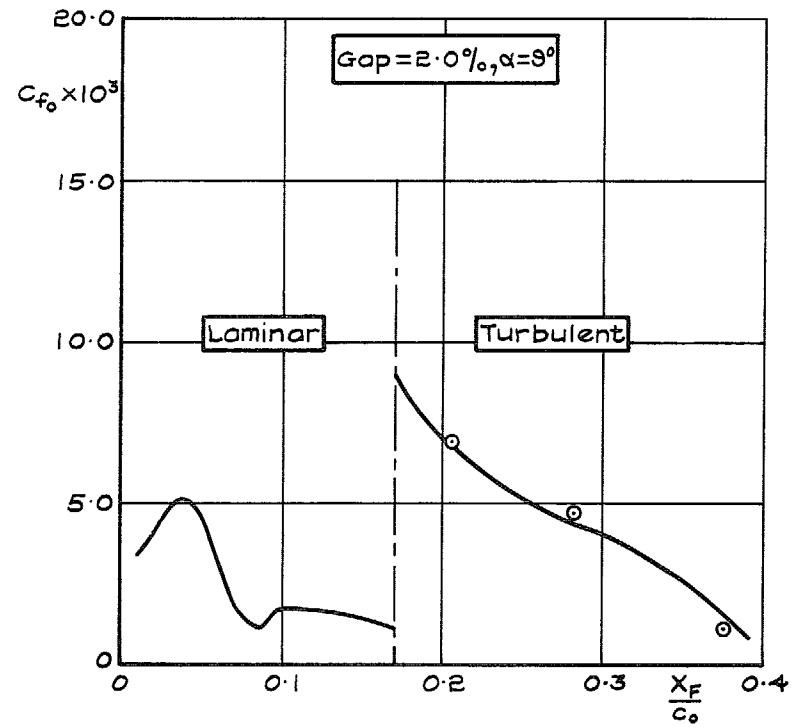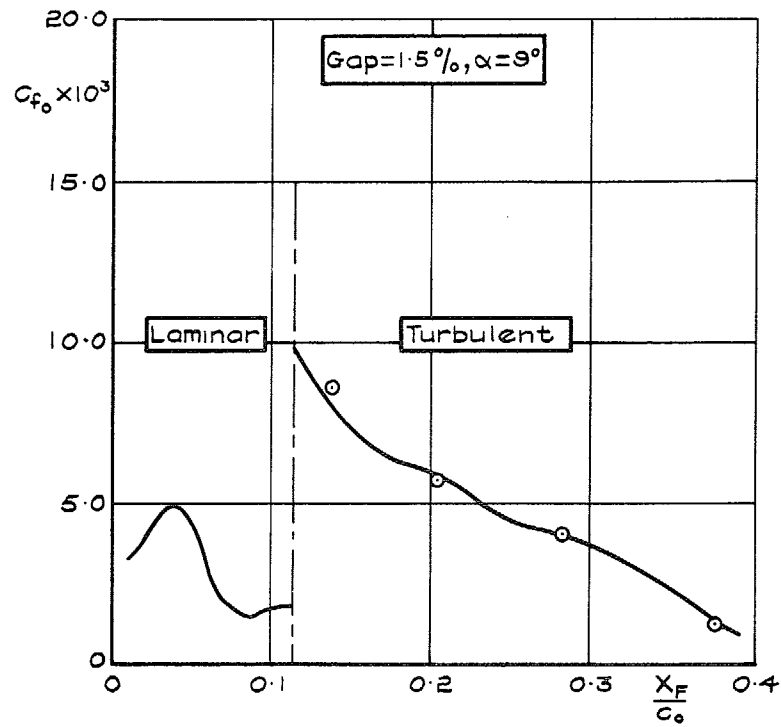
FIG. 43.   Skin-friction coefficient on flap upper surface. Flap deflection 10°.

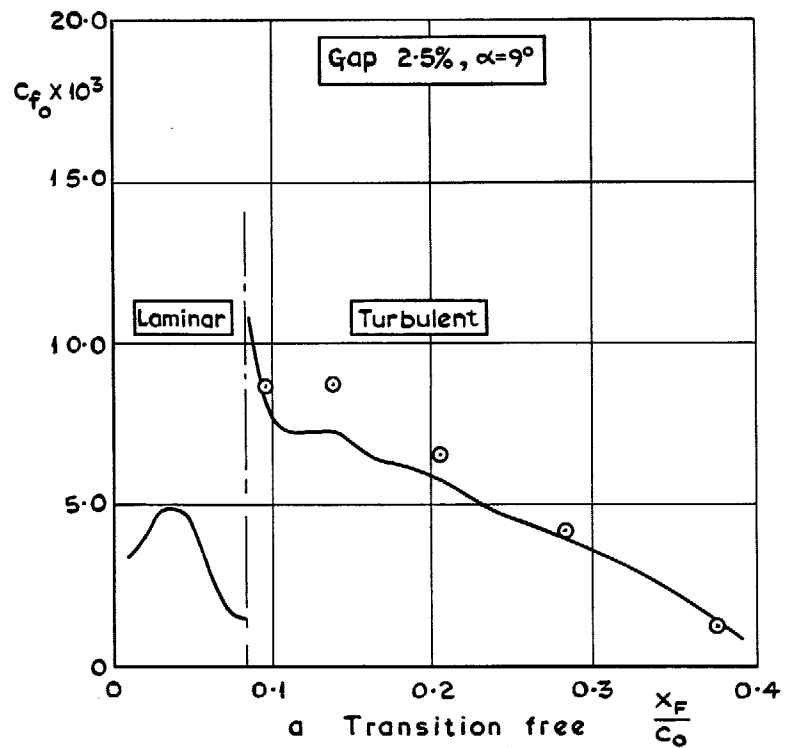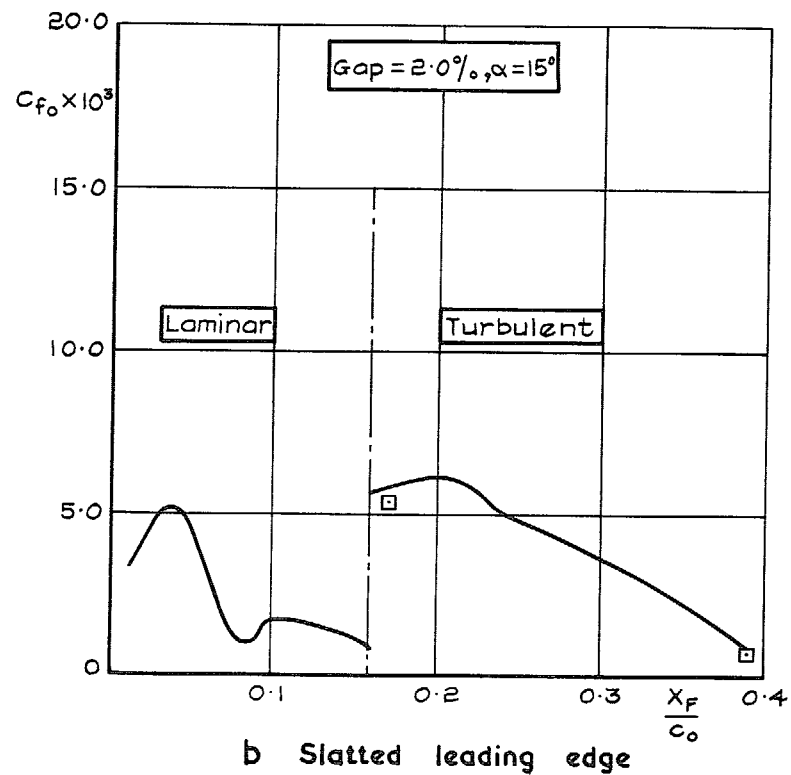| Curve	Symbol	Derivation
	⊙	Measured by razor blade technique
	⊡	Measured by Preston tube
——————		Thwaites' method for laminar flow, Green's method for turbulent flow

a   Transition free

Gap 2·5%, $\alpha = 9°$

Laminar   Turbulent

$C_{f_o} \times 10^3$

b   Transition fixed

Gap = 2·5%, $\alpha = 9°$

Laminar   Turbulent   Separation

$C_{f_o} \times 10^3$
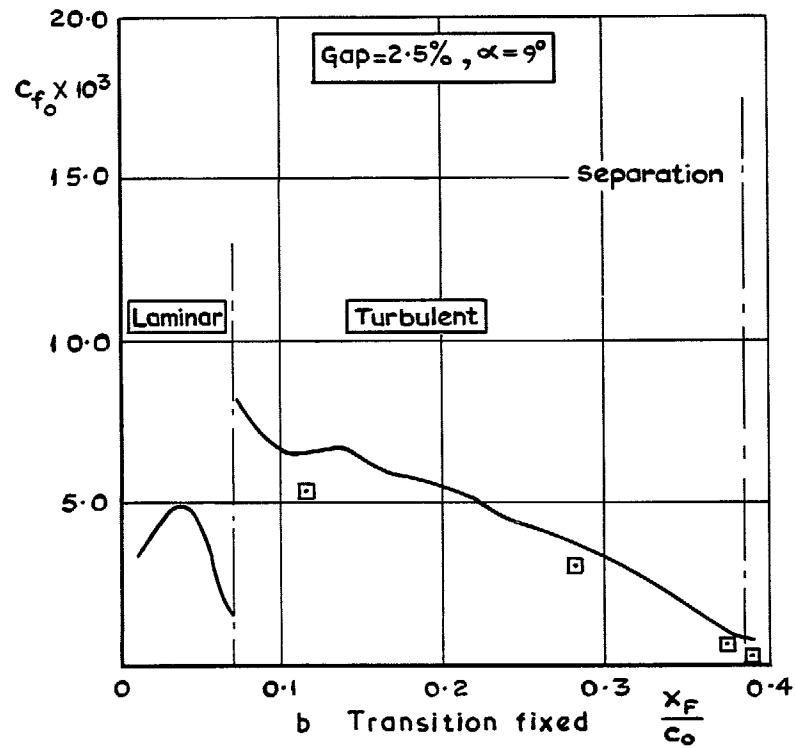
FIG. 44 a. & b.   Comparison of skin-friction coefficient on flap upper surface, transition free and fixed.
Flap deflection 10°.

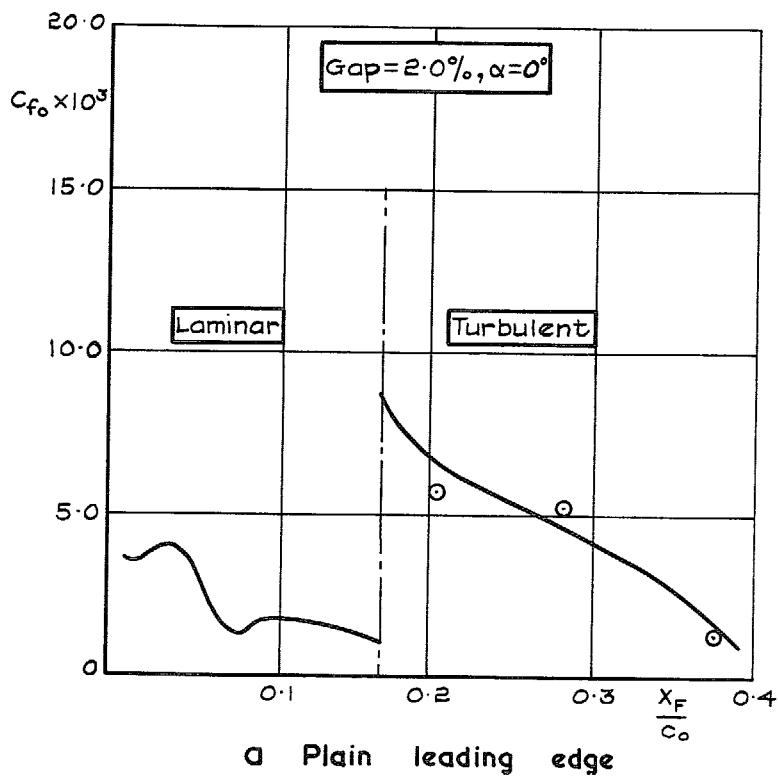| Curve	Symbol	Derivation
	⊙	Measured by razer blade technique
	⊡	Measured by Preston tube
———		Thwaites' method for laminar flow, Green's method for turbulent flow

$Gap = 2.0\%, \alpha = 0°$

Laminar   Turbulent

a   Plain   leading   edge

$Gap = 2.0\%, \alpha = 15°$

Laminar   Turbulent

b   Slatted   leading   edge

FIG. 45 a. & b.   Effect of leading-edge configuration on skin-friction coefficient on flap upper surface.
Flap deflection 10°.